

International  
Progress Report

**IPR-05-31**

# Äspö Hard Rock Laboratory

## Prototype Repository

Acoustic emission and ultrasonic  
monitoring results from deposition  
hole DA3545G01 in the Prototype  
Repository between April 2005  
and September 2005

J.R. Haycox  
W.S. Pettitt  
Applied Seismology Consultants

December 2005

***Svensk Kärnbränslehantering AB***

Swedish Nuclear Fuel  
and Waste Management Co  
Box 5864  
SE-102 40 Stockholm Sweden  
Tel 08-459 84 00  
+46 8 459 84 00  
Fax 08-661 57 19  
+46 8 661 57 19



**Äspö Hard Rock  
Laboratory**



Report no.	No.
<b>IPR-05-31</b>	<b>F63K</b>
Author	Date
<b>J.R. Haycox</b>	<b>December 2005</b>
<b>W.S. Pettitt</b>	
Checked by	Date
<b>Lars-Erik Johannesson</b>	<b>2006-04-24</b>
<b>R.P. Young</b>	
Approved	Date
<b>Anders Sjöland</b>	<b>2006-04-28</b>

# Äspö Hard Rock Laboratory

## Prototype Repository

### Acoustic emission and ultrasonic monitoring results from deposition hole DA3545G01 in the Prototype Repository between April 2005 and September 2005

J.R. Haycox  
W.S. Pettitt  
Applied Seismology Consultants

December 2005

**Keywords:** Field test, Prototype Repository, Acoustic emission, Ultrasonic monitoring, P-wave velocity, S-wave velocity, Rock fractures, Rock properties


This report concerns a study which was conducted for SKB. The conclusions and viewpoints presented in the report are those of the author(s) and do not necessarily coincide with those of the client.



**Report DLV-05-06**

**To  
SKB**

**APPLIED SEISMOLOGY CONSULTANTS**

Last Edited	4 January 2006
File name	SKBProtoHeating to Oct05_25112005.doc
Last Printed	27 April 2006
Signature	



## Executive summary

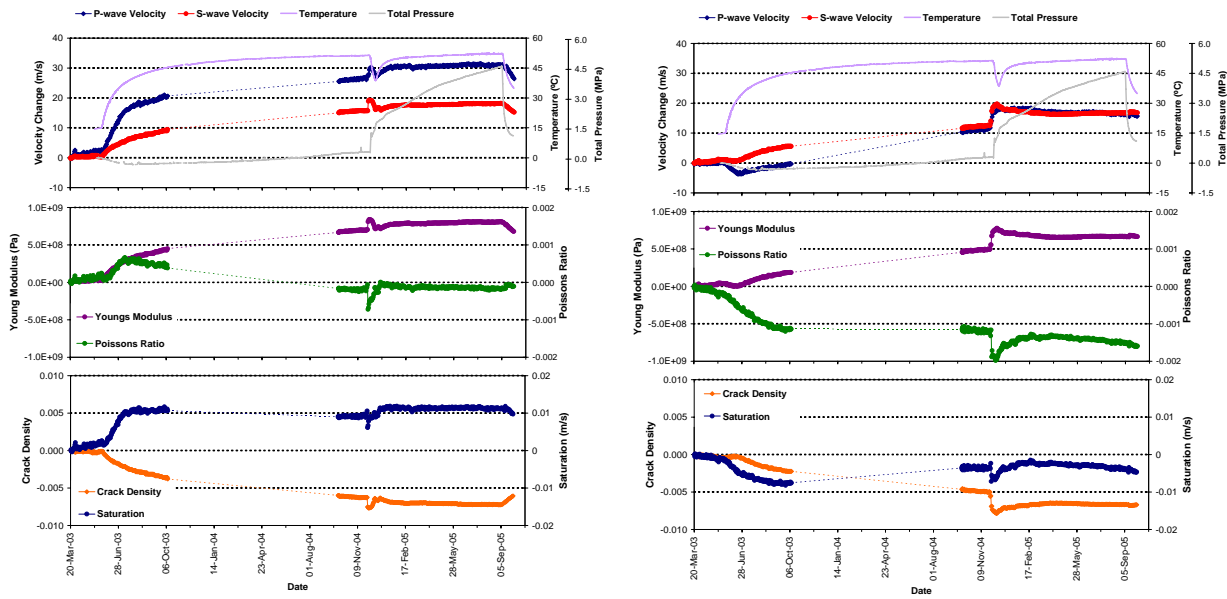
This report describes results from acoustic emission (AE) and ultrasonic monitoring around a canister deposition hole in the Prototype Repository Experiment at SKB's Hard Rock Laboratory (HRL), Sweden. The monitoring aims to examine changes in the rock mass caused by an experimental repository environment, in particular due to thermal stresses induced from canister heating and pore pressures induced from tunnel sealing.

The Prototype Repository Experiment has been designed to simulate a disposal tunnel in a real deep repository for disposal of high-level nuclear waste. Two techniques are utilised here to investigate the processes occurring within the rock mass around the deposition hole. AE monitoring is a 'passive' technique similar to earthquake monitoring but on a much smaller distance scale (source dimensions of millimetres). AEs occur on fractures in the rock when they are created or when they move. Ultrasonic surveys are also used to 'actively' examine the rock. In this case an array of transmitters sends signals to an array of receivers. Amplitude and velocity changes on the ray paths can then be used to examine changes in the rock's properties (Young's modulus, Poisson's ratio, Crack density and Saturation).

AE and Ultrasonic monitoring has previously been conducted at the Prototype Repository during excavation of two deposition holes in Section II of the tunnel and when simulated canisters, installed in the deposition holes, were first heated and the tunnel pressurised. Monitoring is now continuing in 6-monthly reporting periods using a permanent ultrasonic array, with transducers installed into instrumentation boreholes in June 2002, before the tunnel was sealed. In April 2003 heaters in the simulated waste canisters were switched on causing temperatures to rapidly increase in the rock mass up to approximately 50°C at the rock wall. In November 2004 water drainage from the sealed Prototype tunnel was stopped causing a rapid increase in fluid pressures in the deposition hole.

This report relates to the monitoring period starting 1<sup>st</sup> April 2005. During this period the temperature increases at a constant slow rate until 5<sup>th</sup> September 2005. After this date there is an exponential decrease consistent with the turning off of heaters in the deposition hole. Similarly, there is a trend of increasing pressure up to 5<sup>th</sup> September Repository.

Velocity changes are measured between transmitter-receiver pairs on the daily ultrasonic surveys using a cross-correlation technique that allows a velocity resolution of  $\pm 2\text{m.s}^{-1}$ . Relative to previous monitoring, there is only a small change in average velocity recorded during the monitoring period (averaged over all ray paths), with a general decrease observed when temperature and pressure starts to decrease. The velocity results on individual ray paths show that the largest decreases during cooling and depressurisation are occurring on raypaths passing through a region of low compressive stress (or slightly tensile stress) described by three-dimensional elastic stress modelling performed by *Pettitt et al.* [2000]. P-wave velocity shows a greater degree of variation than S-wave velocity. Amplitude changes are also relatively small during this reporting period. P-wave amplitudes are relatively constant until 5<sup>th</sup> September 2005, when there is a systematic decrease associated with the cooling and depressurisation. S-wave amplitudes increase slightly during the first part of the reporting period followed by a decrease that follows a similar trend to the P-waves.



**Velocity and modulus change for raypaths passing close to the deposition hole through the tensile zone (left) and the compressive zone (right).**

Calculated rock parameters (Young's Modulus, Poisson's Ratio, Crack Density and Saturation) show that ray paths that pass at distance from the deposition hole pass through rock that is relatively unaffected by the reduction in temperature and pressure. Greater variation is observed on raypaths that pass through regions of high and low compressive stress zones respectively, close to the deposition hole wall. An increase in crack density is observed in the region of low compressive stress, which is interpreted as the opening of existing microfractures and pore spaces. During the period of cooling and de-pressurisation, saturation is observed to decrease on raypaths through zones of both the high and low compressive stress, possibly as a result of the combined effect of lowering fluid pressures whilst the rock remains relatively warm ( $>35^{\circ}\text{C}$ ).

Significant differences have been observed in the response on raypaths passing through volumes of rock in states of high and low compressive stresses induced by the *in situ* stress field and the deposition hole void. Raypaths that pass through unloaded volumes of the rock mass record a much higher response and are more sensitive to thermal stresses, caused by changes in temperature, than ray paths that pass through loaded volumes. Measured changes in velocities and amplitudes, and calculated rock parameters, are a result of the three-dimensional stress state of the rock around the deposition hole and the coupled nature of the pressure and temperature effects in the loaded and unloaded volumes. It's observed that since drainage from the Prototype Repository was closed in November 2004 pressure from within the deposition hole, caused by hydraulic pressure and swelling of the bentonite buffer, is the primary constraint on these changes. The pressure increase acts as a confining pressure on the rock mass leading to a closure of the pre-existing microcrack fabric and so a reduction in crack density. We observe that only a relatively small pressure increase is sufficient to close this microcrack fabric in the volumes already under high compressive stresses, leading to an initially high rate of change in measured velocities followed by a constant level, even though pressures and temperatures may keep increasing afterwards. The required pressure increase is approximately 1.5MPa. Volumes of rock that have high



compressive stresses, induced from the *in situ* stress field, and have high confining pressure from the deposition hole interior have a relatively closed microcrack fabric leading to a relative insensitivity to changing thermal stresses. Volumes of rock that have low compressive stresses record a relatively high response to the change in temperature as the microcrack fabric in these volumes is relatively unconfined allowing the fabric to be reactive to an unloading of thermal stresses.

Thirty-eight AEs have been located with high confidence from 82 triggered events recorded during the monitoring period. The rate of activity increases slightly in early September co-incident with the pressure and temperature decreases. The majority of the AEs locate in the immediate vicinity of deposition hole DA3545G01. Two events also locate close to the neighbouring deposition hole DA3551G01. The events observed here are consistent with the results from previous monitoring with the small amount of clustering observed locating in regions of previous activity. The events are therefore interpreted as a continuation of activity in the previously imaged damage zone and, similar to during excavation and initial heating, are created either by movement on pre-existing microcracks, or as a result of extension or formation of new microcracks in the existing damaged region. Four events are located in the rock mass between the two deposition holes at between 455.3 and 455.7m depth. The events are believed to coincide with a semi-horizontal macroscopic fracture that is observed to intersect the deposition holes at this height and are consistent with similar events recorded during the excavation and heating phases.

The frequency of located events during this reporting period is low compared to when temperature was increasing at a faster rate and when the rapid change in pressure occurred in December 2004. The low number of AEs suggests the rock mass has stabilised. The primary contribution to this is believed to be the confining pressure applied from the deposition hole producing a cessation in AEs as movement on macrofractures and microcracks is inhibited; a response observed in laboratory rock tests and in the Tunnel Sealing Experiment (TSX) at AECL's Underground Research Laboratory (URL). At the end of the reporting period the rapid decrease in temperature and pressure appears to have little affect on the number, or distribution of AEs around the deposition hole, although the rate may be slowly accelerating at the end of the monitoring period. This suggests that the environmental changes have caused no redistribution of stresses sufficient to re-initiation further significant microfracturing.



# Contents

<b>Executive summary</b>	<b>5</b>
<b>Contents</b>	<b>9</b>
<b>Table of Figures</b>	<b>11</b>
<b>Table of Tables</b>	<b>14</b>
<b>1 Introduction</b>	<b>15</b>
<b>2 Specific Objectives</b>	<b>19</b>
<b>3 Previous Monitoring at the Prototype Repository</b>	<b>21</b>
<b>4 Results</b>	<b>25</b>
4.1 Ultrasonic surveys	25
4.2 Acoustic Emissions	40
<b>5 Summary of Monitoring to Date</b>	<b>47</b>
<b>6 Results Summary and Conclusions</b>	<b>61</b>
6.1 Overview	61
6.2 Ultrasonic Surveys	62
6.3 Acoustic Emissions	63
<b>References</b>	<b>65</b>
<b>Appendix I Methodology</b>	<b>67</b>
<b>Appendix II Processing Parameters</b>	<b>75</b>



# Table of figures

<b>Figure 1-1:</b> Plan view of the experimental tunnels at the Äspö HRL and the location of the Prototype Repository. A schematic illustration of the final experimental set up is shown with canisters and bentonite clay buffer installed in the 1.75m diameter deposition holes. Note the entrance of the tunnel is towards the left. Graphics are modified from SKB[1999].	16
<b>Figure 1-2:</b> Temperature (TR instruments) measured in the rock adjacent to the deposition hole and total pressure (PB and UB instruments) measured on the rock wall. Total pressure is the sum of pore pressure and bentonite swelling pressure [Goudarzi, 2005].	17
<b>Figure 3-1:</b> Ultrasonic results and modulus results for raypath transmitter 1 to receiver 6 during excavation (left) and heating (right).	22
<b>Figure 3-2:</b> Projections of all AEs located during the heating phase. Events are scaled to instrument magnitude.	23
<b>Figure 4-1:</b> Lower-hemisphere stereonet of a) P-wave velocity and b) S-wave velocity for the reference survey on 8 <sup>th</sup> December 2004. The ray path orientations are shown by black markers.	25
<b>Figure 4-2:</b> Temperature around deposition hole DA3545G01. The sensors are positioned mid-way up the deposition hole with different depths into the rock mass (see right-hand inset) [Goudarzi, 2005].	27
<b>Figure 4-3:</b> Total pressure in (a) the backfill over deposition hole DA3545G01; and (b) in the rock adjacent to deposition hole DA3545G01 [Goudarzi, 2005].	28
<b>Figure 4-4:</b> Average P- and S-wave (a) velocity change, and (b) amplitude change, for the reporting period. Temperature (TR6045) and total pressure (PB616) are displayed on the secondary axes.	29
<b>Figure 4-5:</b> Example plots of (a) raw waveform data points and (b) cross correlation windows for the raypath transmitter 7 to receiver 2. The second plot also shows the reference survey from 8 <sup>th</sup> December 2004.	30
<b>Figure 4-6:</b> Interpretation of the ultrasonic results during excavation in terms of disturbed and damaged regions around the deposition hole. Zones of induced stress are inferred from elastic modelling and the $\sigma_1$ orientation. After Pettitt et al.[1999].	32
<b>Figure 4-7:</b> Velocity changes measured on ray path category 'S3' (Figure 4-6) for deposition hole DA3545G01. Ray paths shown are from a top transmitter to receivers with increasing depth: a) transmitter, $t_n=1$ , receiver, $r_n=5$ ; b) $t_n=1$ , $r_n=6$ ; c) $t_n=1$ , $r_n=7$ ; d) $t_n=4$ , $r_n=2$ . Schematic diagrams in the right margin indicate the relative locations of transmitter (red) and receiver (gold). Temperature (TR6045) is displayed on the secondary axes.	34

- Figure 4-8:** Velocity changes measured on ray path category 'S1' (Figure 4-6) for deposition hole DA3545G01. Ray paths shown are from a top transmitter to receivers with increasing depth: a) transmitter,  $t_n=7$ , receiver,  $r_n=5$ ; b)  $t_n=7$ ,  $r_n=6$ ; c)  $t_n=7$ ,  $r_n=7$ ; d)  $t_n=7$ ,  $r_n=8$ . Schematic diagrams in the right margin indicate the relative locations of transmitter (red) and receiver (gold). Temperature (TR6045) is displayed on the secondary axes. 35
- Figure 4-9:** Raypaths showing a significant decrease (greater than  $4\text{m}\cdot\text{s}^{-1}$ ) after 5<sup>th</sup> September 2005 for A) P-wave velocity and B) S-wave velocity. The upper plots are viewed northwards, the lower plots are viewed just off the vertical. 36
- Figure 4-10:** Velocity change plots of 5 raypath categories around deposition hole DA3545G01 for (a) P-waves and (b) S-waves. Temperature (TR6045) and total pressure (PB616) are displayed on the secondary axes. 37
- Figure 4-11:** Amplitude change plots of 5 raypath categories around deposition hole DA3545G01 for (a) P-waves and (b) S-waves. Temperature (TR6045) and total pressure (PB616) are displayed on the secondary axes. 38
- Figure 4-12:** Modulus during this reporting period for average P- and S-wave velocity values on different raypath orientations. (a) Young's Modulus, (b) Poisson's Ratio, (c) Crack Density and (d) Saturation. Raypath orientations are described in Figure 4-6. Temperature (TR6045) and total pressure (PB616) are displayed on the secondary axes. 39
- Figure 4-13:** Temporal response plot of (a) AE triggers and (b) located AEs; number per day on left axes and cumulative number right hand axes. 42
- Figure 4-14:** Three views of AE activity located around deposition holes DA3545G01 and DA3551G01. (Top: Oblique view looking North. Middle: Transverse view looking north. Bottom: Plan view). A cluster, further discussed in the text, is marked i. 43
- Figure 4-15:** Waveforms from selected events shown in relation to a transverse view of AE activity. 44
- Figure 4-16:** Plan view of AEs located around deposition hole DA3545G01 during (a) the excavation phase, and (b) this reporting period. The red arrows mark the orientation of the principle stress. 45
- Figure 5-1:** P- and S-wave (a) velocity change and (b) amplitude change from the start of monitoring, plotted alongside temperature (TR6045) and pressure (PB616) measurements in deposition hole DA3545G01. The vertical blue lines represents the end of the previous reporting period and the start of this reporting period. 50
- Figure 5-2:** Average P- and S-wave velocity change for raypaths on category 'S1' together with temperature (TR6045) and total pressure (PB616) (top), Young's Modulus and Poisson's Ratio change (middle), and Crack Density and Saturation change (bottom). 51

<b>Figure 5-3:</b> Average P- and S-wave velocity change for raypaths on category ‘S3’ together with temperature (TR6045) and total pressure (PB616) (top), Young’s Modulus and Poison’s Ratio change (middle), and Crack Density and Saturation change (bottom).	52
<b>Figure 5-4:</b> Average P- and S-wave velocity change for raypaths on category ‘C1’ together with temperature (TR6045) and total pressure (PB616) (top), Young’s Modulus and Poison’s Ratio change (middle), and Crack Density and Saturation change (bottom).	53
<b>Figure 5-5:</b> Average P- and S-wave velocity change for raypaths on category ‘C2’ together with temperature (TR6045) and total pressure (PB616) (top), Young’s Modulus and Poison’s Ratio change (middle), and Crack Density and Saturation change (bottom).	54
<b>Figure 5-6:</b> Average P- and S-wave velocity change for raypaths on category ‘Far’ together with temperature (TR6045) and total pressure (PB616) (top), Young’s Modulus and Poison’s Ratio change (middle), and Crack Density and Saturation change (bottom).	55
<b>Figure 5-7:</b> Average amplitude change for raypaths passing through the deposition hole, together with temperature (TR6045) and total pressure (PB616).	57
<b>Figure 5-8:</b> (a) Number and cumulative number of located events from the start of monitoring, (b) average number of AE events per day (averaged over 17 days) and (c) temperature (TR6045) and pressure (PB616) measurements in deposition hole DA3545G01.	58
<b>Figure 5-9:</b> Schematic diagram of the deposition hole and explanation of changes experienced during Phase 1.	59
<b>Figure 5-10:</b> Schematic diagram of the deposition hole and explanation of changes experienced during Phase 2.	59
<b>Figure 5-11:</b> Schematic diagram of the deposition hole and explanation of changes experienced during Phase 3.	60
<b>Figure 6-1 (Appendix 1):</b> Top: Schematic diagram of the locations of all transducers on a single frame. Left: Photo of a section of the transducer assembly. Right: The transducer assembly during installation.	68
<b>Figure 6-2 (Appendix 1):</b> Plan view of the array geometry for Deposition Hole DA3545G01 during heating in the Prototype Tunnel. The blue solid lines represent direct raypaths between sondes illustrating their ‘skimming’ nature. The blue dashed line represents a raypath that travels through the deposition hole.	69
<b>Figure 6-3 (Appendix 1):</b> Schematic diagram of the hardware used for the heating stage in the Prototype Repository. The ultrasonic pulse generator sends a signal to each transmitter and the resulting signal is recorded on each receiver. The receivers are also used to listen for AE activity. The archive PC is required to make a copy of the data for backup purposes.	70

**Figure 6-4 (Appendix 1):** Waveforms recorded from one transmitter on the array of sixteen receivers. The gold markers indicate the transmission time. The blue and green markers indicate picked P- and S-wave arrivals respectively. 71

**Figure 6-5 (Appendix 1):** Locations of calibration shots obtained from a series of tests at 1 metre intervals down the wall of deposition hole DA3545G01. The two views show that these line up and are located close to the surface of the hole. 74

**Figure 6-6 (Appendix 1):** Example waveforms from each of the 16 receiving channels for a ‘pencil-lead break’ test undertaken against the Deposition Hole (DA3545G01) wall 6 metres below the tunnel floor. 74

## Table of tables

**Table 5-1 (Appendix 1):** Summary of velocity, amplitude and AE variation measured during three periods of temperature and/or pressure change. 56

**Table 6-1 (Appendix 1):** Boreholes used for AE monitoring of deposition hole DA3545G01. 69



# 1 Introduction

This report describes results from acoustic emission (AE) and ultrasonic monitoring around a canister deposition hole (DA3545G01) in the Prototype Repository Experiment at SKB's Hard Rock Laboratory (HRL), Sweden. The monitoring aims to examine changes in the rock mass caused by an experimental repository environment, in particular due to thermal stresses induced from canister heating and pore pressures induced from tunnel sealing. Monitoring of this volume has previously been performed during excavation [Pettitt *et al.*, 1999] and during the initial stages of canister heating and tunnel pressurisation [Haycox *et al.*, 2005]. This report is the first of an ongoing 6-monthly processing and interpretation of the results for the experiment and relates to the period between 1<sup>st</sup> April 2005 and 30<sup>th</sup> September 2005.

The Prototype Repository Experiment (Figure 1-1) has been designed to simulate a disposal tunnel in a real deep repository for disposal of high-level nuclear waste. Its objective is 'to test and demonstrate the integrated function of the repository components under realistic conditions on a full scale and to compare results with models and assumptions'. The experiment consists of a 90m long, 5m diameter sub-horizontal tunnel excavated in a dioritic granite using a Tunnel Boring Machine (TBM). The rock mass has two main discontinuous sets of sparse, en-echelon fractures [Patel *et al.*, 1997]. The Prototype Repository design incorporates six full-scale canister deposition holes which have been excavated vertically into the floor of the tunnel using a TBM converted to vertical boring. Each deposition hole measures 1.75m in diameter and approximately 8.8m in length. Simulated waste canisters, encased in a bentonite buffer, have been placed into each deposition hole and heated from within by specially designed electric heaters to simulate disposed nuclear material. The tunnel was then backfilled using a mixture of bentonite and crushed rock, and sealed using concrete plugs.

AE and ultrasonic monitoring is one of a number of scientific measurements being used to remotely monitor the performance of the Prototype Repository. The locations and results from temperature, total-pressure, pore water pressure and water saturation instruments are presented separately (see Goudarzi and Johannesson[2004]). These measurements are used in this report to assist in the interpretation of the ultrasonic results. In particular, temperature and total pressure measured on the rock wall of the deposition hole (Figure 1-2) are related to significant changes that are observed in the ultrasonic measurements. This data is provided by Goudarzi[2005].

AE and ultrasonic monitoring is a tool for remotely examining the extent and severity of damage and disturbance around an excavation. This can be induced by the excavation method itself, by the redistribution of stresses (loading or unloading) resulting from the void or by environmental effects such as heating, saturation or pressurisation. Acoustic techniques are particularly adept at assessing the Excavation Damaged or Disturbed Zone (EDZ) as they allow it to be mapped spatially and temporally with high resolution, and they allow the effect on the rock mass to be quantifiably measured. Furthermore, acoustic techniques allow investigations to be conducted remotely, without the need for potentially damaging coring. Young and Pettitt [2000] give a review of AE and ultrasonic results from a number of experiments conducted in different underground environments.

- AE monitoring is a ‘passive’ technique similar to earthquake monitoring but on a much smaller distance scale (source dimensions of millimetres). AEs occur on fractures in the rock sample when they are created or when they move. The data acquisition system triggers on AEs when they occur and records full-waveform information that can then be used to delineate the amount, time, location and mechanism of fracturing.
- Ultrasonic surveys are used to ‘actively’ examine the rock. In this case an array of transmitters sends signals to an array of receivers. Amplitude and velocity changes on the ray paths can be interpreted in terms of changes in the material properties of the rock. Calculations using the velocities can determine the dynamic moduli, Young’s modulus and Poisson’s ratio, to give direct indications of the properties of the rock through which the raypaths travel. Crack density and saturation can also be calculated to determine changes in crack properties in the damaged and disturbed zones.

Detailed descriptions of the data acquisition and processing methodology are presented in Appendix I. The ultrasonic array consists of twenty-four ultrasonic transducers configured as eight transmitters and sixteen receivers installed into four instrumentation boreholes using specially designed installation frames sealed within slightly expansive grout. The array is designed to provide good coverage for AE locations and provide ‘skimming’ ray paths so as to sample the rock immediately adjacent to the deposition hole wall. ASC’s InSite Seismic Processor [Pettitt *et al.*, 2005], has been used to automatically process both the AE and ultrasonic survey data. Appendix II A and Appendix II B give the processing parameters used. Data from daily ultrasonic surveys has been automatically picked and arrivals cross-correlated to a reference survey for high-precision measurements of P- and S-wave velocity change through the experiment. Arrivals of AEs have been manually picked and three dimensional source locations have been calculated.

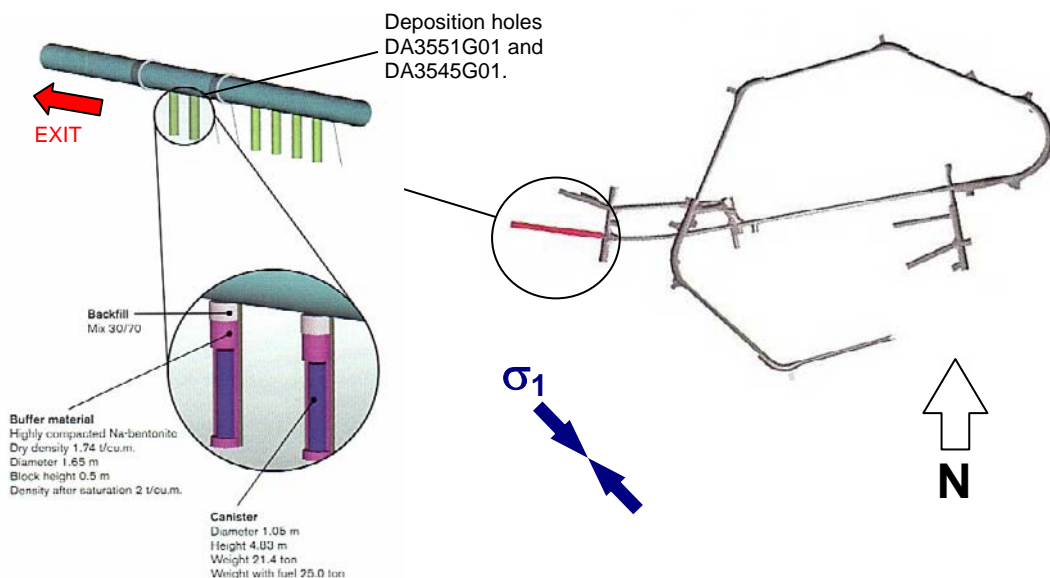


**Figure 1-1:** Plan view of the experimental tunnels at the Äspö HRL and the location of the Prototype Repository. A schematic illustration of the final experimental set up is shown with canisters and bentonite clay buffer installed in the 1.75m diameter deposition holes. Note the entrance of the tunnel is towards the left. Graphics are modified from SKB[1999].

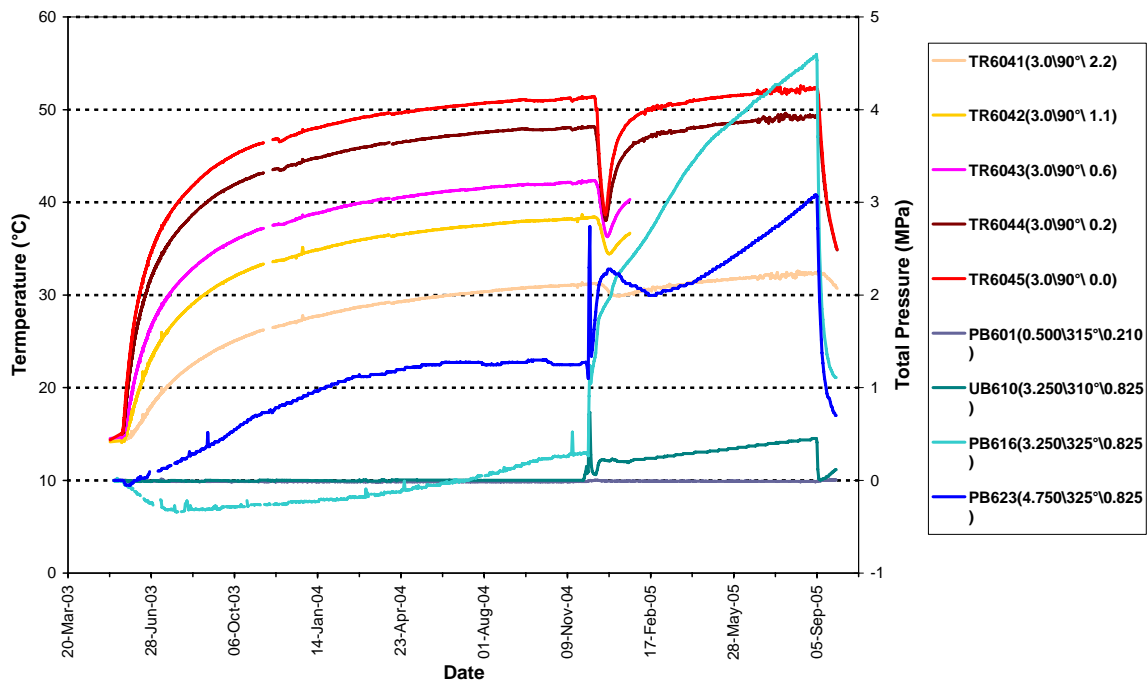


**Figure 1-2:** Temperature (TR instruments) measured in the rock adjacent to the deposition hole and total pressure (PB and UB instruments) measured on the rock wall. Total pressure is the sum of pore pressure and bentonite swelling pressure [Goudarzi, 2005].



## 2 Specific Objectives

This six-month period of ultrasonic monitoring in the Prototype Repository Experiment, has been undertaken with the following objectives:

- Produce accurate source locations for AEs so as to delineate the spatial and temporal extent of any brittle microcracking within the rock mass around the deposition hole and locate any movements on pre-existing macroscopic fractures.
- Conduct regular ultrasonic surveys to assess the effect of heating and other environmental changes on the velocity and amplitude of transmitted ultrasonic waves.
- Investigate changes in dynamic moduli and crack density to show how the properties of the rock volume around the deposition hole change through the experiment.
- Relate the AE and ultrasonic measurements to the measured *in situ* stress regime and other operating parameters such as temperature and fluid pressure.
- Outline how the results from this reporting period relate to previous monitoring periods, and into the overall experimental aims and objectives.



### 3 Previous Monitoring at the Prototype Repository

Ultrasonic monitoring has been conducted at the Prototype Repository during excavation of two deposition holes, and during initial heating and pressurisation leading up to 31<sup>st</sup> March 2005. This report presents new results from the period 1<sup>st</sup> April to 30<sup>th</sup> September 2005.

A temporary ultrasonic array was installed around the rock volume when deposition hole DA3545G01 and its neighbour DA3551G01 were first excavated in September 1999 [Pettitt *et al.*, 1999]. A total of 2467 AE triggers were obtained during monitoring of the two deposition holes. Of these 1153 were located. There was significantly more AE activity around the second deposition hole (labelled DA3545G01) than the first (DA3551G01). This difference is likely to depend upon intersection of the excavation with a greater number of pre-existing fractures. These fractures may be preferentially located in the side wall of the deposition hole or preferentially orientated to the *in situ* stress field. Fracturing associated with excavation-induced stresses was observed with AEs distributed mainly in regions orthogonal to the maximum principal stress,  $\sigma_1$ . This was consistent with observations from the Canister Retrieval Tunnel and from dynamic numerical models. AEs, and hence microcrack damage, were shown to locate in clusters down the deposition hole and not as a continuous 'thin skin'. Pettitt *et al.*[2000] showed that these clusters were associated with weaknesses in the rock mass generated by excavation through pre-existing fractures. Damage in the side wall of the deposition holes depended significantly on these pre-existing features. The *in situ* stress field was a contributing factor in that induced stresses were sufficiently high to create damage in these weakened regions although not sufficiently high to create significant damage in the rock mass as a whole.

A permanent ultrasonic array, with transducers grouted into instrumentation boreholes, was installed in the rock mass in June 2002. Ultrasonic monitoring has been conducted in two periods between 20<sup>th</sup> March and 9<sup>th</sup> October 2003, and from 29<sup>th</sup> September 2004. The gap in monitoring occurred when the ultrasonic acquisition system was used for another experiment in the HRL (Pillar Stability Experiment). Haycox *et al.*[2005] processed and reported results for these two periods. In April 2003 heaters in the simulated waste canister were switched on causing temperatures to rapidly increase in the rock mass up to approximately 50°C at the rock wall. In November 2004 water drainage from the sealed Prototype tunnel was ceased causing a rapid increase in fluid pressures.

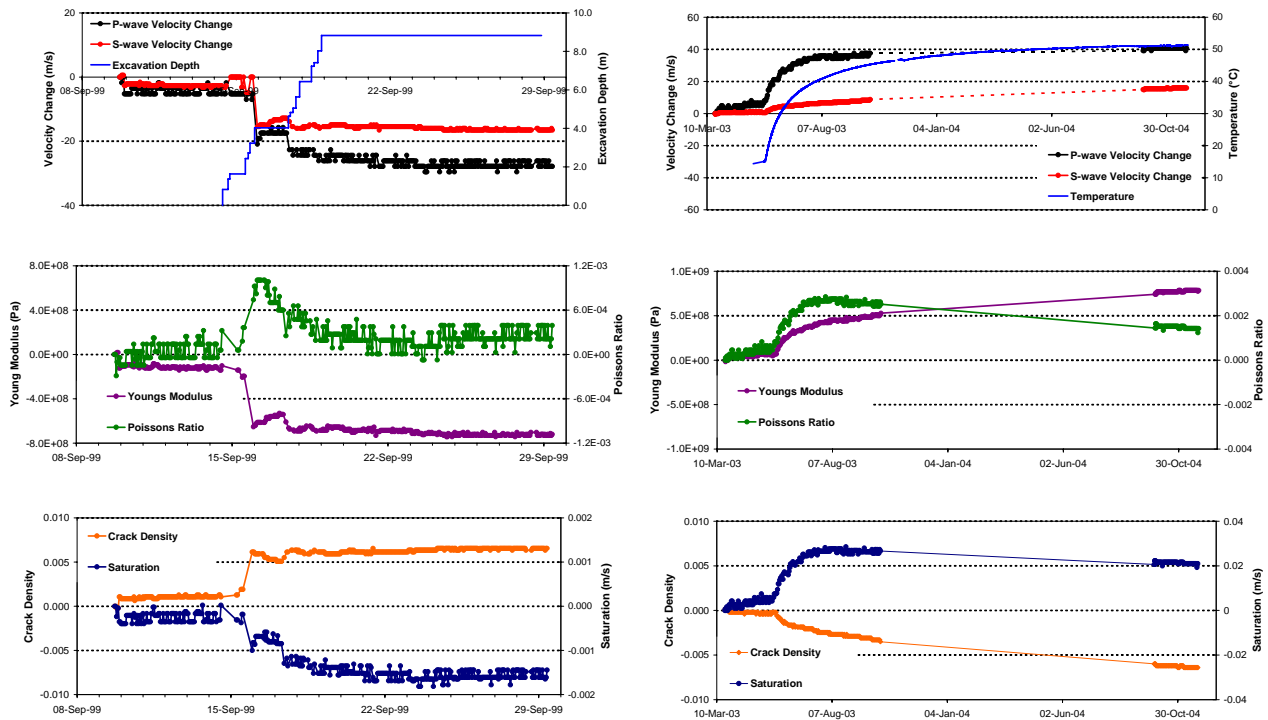


**Figure 3-1:** Ultrasonic results and modulus results for raypath transmitter 1 to receiver 6 during excavation (left) and heating (right).

The majority of processed raypaths during the heating period showed consistent behaviour, with the general trend being an increase in signal velocities and amplitudes for both P- and S-waves. The velocity changes related to an increase in Young's Modulus during the heating period (indicating the rock gets gradually stiffer) and a reduction in Crack Density as cracks closed. The closure of microcracks and pore spaces in the excavation damaged zone and surrounding stress-disturbed volumes indicated that thermal stresses were acting to increase the compressive stresses around the deposition hole.

Ultrasonic measurements showed that the low-compressive stress, or tensile, region induced by the *in situ* stress field around the excavation void was more responsive to heating, exhibiting rapid increases in P- and S-wave velocity. The high-compressive zone also exhibited increases in velocity, but both P and S-wave velocities responded slower in the first few months. The difference in the rate of response between the two raypath categories was interpreted as a different magnitude of response of the microfractures in the rock mass to increasing thermal stresses. In the low-compressive region, existing microfractures were initially unloaded and hence more open than similar microfractures in the compressive region, where stresses acted to clamp the fractures. As thermal stresses were applied to the rock mass the open fractures were more sensitive to the stress increase and hence responded to a greater extent, and far quicker, than those that were pre-clamped, resulting in more responsive ultrasonic signals. Figure 3-1 compares velocity, amplitude and modulus changes along a single raypath between excavation and heating. The raypath passes through a possible region of tensile fracturing. P- and S-wave velocities decrease a similar amount during excavation as they increase during heating. This suggests very strongly that the microfractures induced in the regions of tensile damage around the deposition hole close when thermal stresses are applied.



An increase in pressure induced in the Prototype at the end of November 2004 resulted in significant changes to the character of many recorded waveforms from the ultrasonic surveys. This suggests that as pressure is increased in the rock surrounding the deposition hole, attenuation of the ultrasonic waves is significantly reduced meaning that they can pass more efficiently through the rock medium. The reduction in attenuation is either a result of an increase in saturation in the rock mass (fluids are pushed into microcracks and pore spaces), or a result of a reduction in crack density caused by a closing of pre-existing microcracks, or a combination of the two.

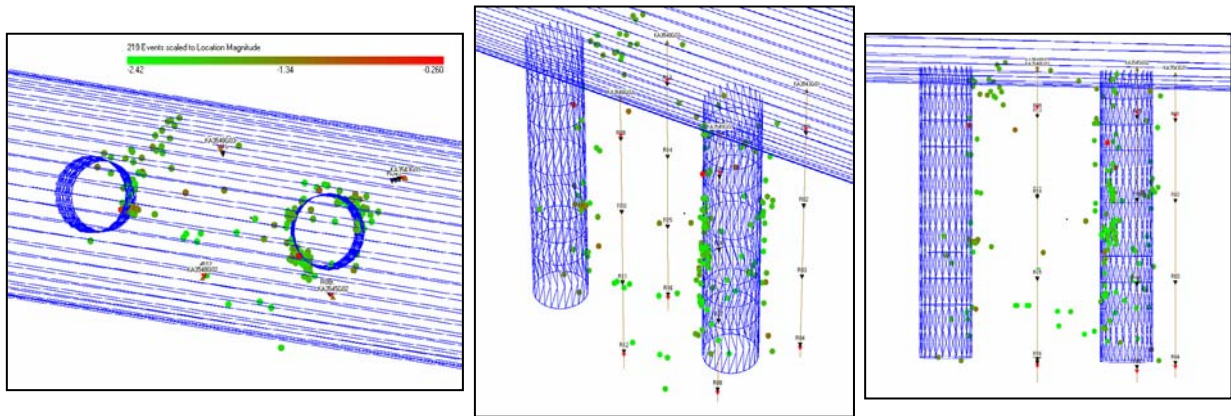


**Figure 3-2:** Projections of all AEs located during the heating phase. Events are scaled to instrument magnitude.

219 events were located with high confidence during the whole reporting period. Figure 3-2 shows the location of the AE's in relation to the deposition holes and tunnel. The majority of the events located close to the deposition hole wall, within the first 20cm and were distributed in the NE and SW quadrants that coincided with regions of increased compressive stress induced by the interaction of the stress field with the excavation void. This activity was interpreted as stress disturbance of the rock mass, particularly around pre-existing macrofractures that commonly intersect the excavation, or microcracking in the immediate vicinity of the fractures. The peak rate of observed AE activity coincided with the rapid changes in pressure in the Prototype. A peak of 32 events occurred on 5<sup>th</sup> December 2004, when pressure in the buffer was highest, with events predominantly locating around deposition hole DA3545G01. The increase in activity was the result of stress changes in the rock around the deposition hole associated with this relatively sudden increase in pressure. The stress changes were inducing small scale movements on pre-existing microfractures created during excavation, or were inducing new microfractures in weaker volumes of the rock. Pore pressure increases may also have assisted in inducing slip on pre-existing microfractures, by reducing the normal stress on the fractures.



## 4 Results

### 4.1 Ultrasonic surveys

Figure 4-1 shows the three-dimensional velocity structure for the survey recorded on 8<sup>th</sup> December 2004. This has been used as the reference survey for processing ultrasonic results for this monitoring period. The survey was performed after the rapid change in pressure in the deposition hole that occurred on 4<sup>th</sup> December 2004. The reference survey is recognised as containing some of the best quality signals so far recorded during the experiment and has one of the largest average amplitudes, thus enabling the highest number of possible raypaths to be processed. Raypaths passing through the deposition hole have been removed.

A total of 80 ray paths have been processed from the reference survey for P-wave velocities (Figure 4-1a) and 49 for S-wave velocities (Figure 4-1b). At this time in the experiment, the structure is principally isotropic but with some localised heterogeneities. These are caused by a combination of measurement uncertainty (estimated at  $\pm 30\text{m.s}^{-1}$  for absolute velocity measurements) and localised effects from the deposition hole (excavation damage zone and stress field). The average P-wave velocity is  $5985\text{m.s}^{-1}$  and the average S-wave velocity is  $3343\text{m.s}^{-1}$ . This is significantly faster than in March 2003, before heating and pressurisation, which showed an average P-wave velocity of  $5909\text{m.s}^{-1}$  and an average S-wave velocity of  $3315\text{m.s}^{-1}$ .

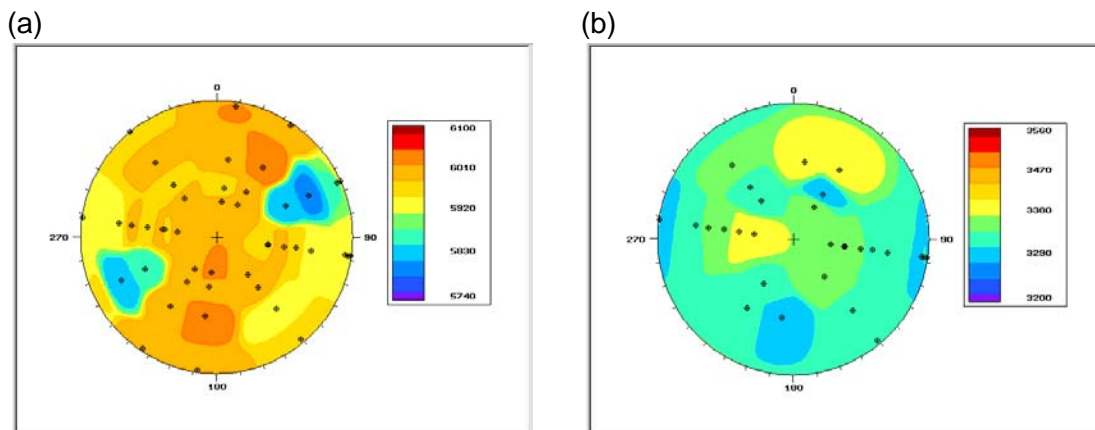


**Figure 4-1:** Lower-hemisphere stereonets of a) P-wave velocity and b) S-wave velocity for the reference survey on 8<sup>th</sup> December 2004. The ray path orientations are shown by black markers.

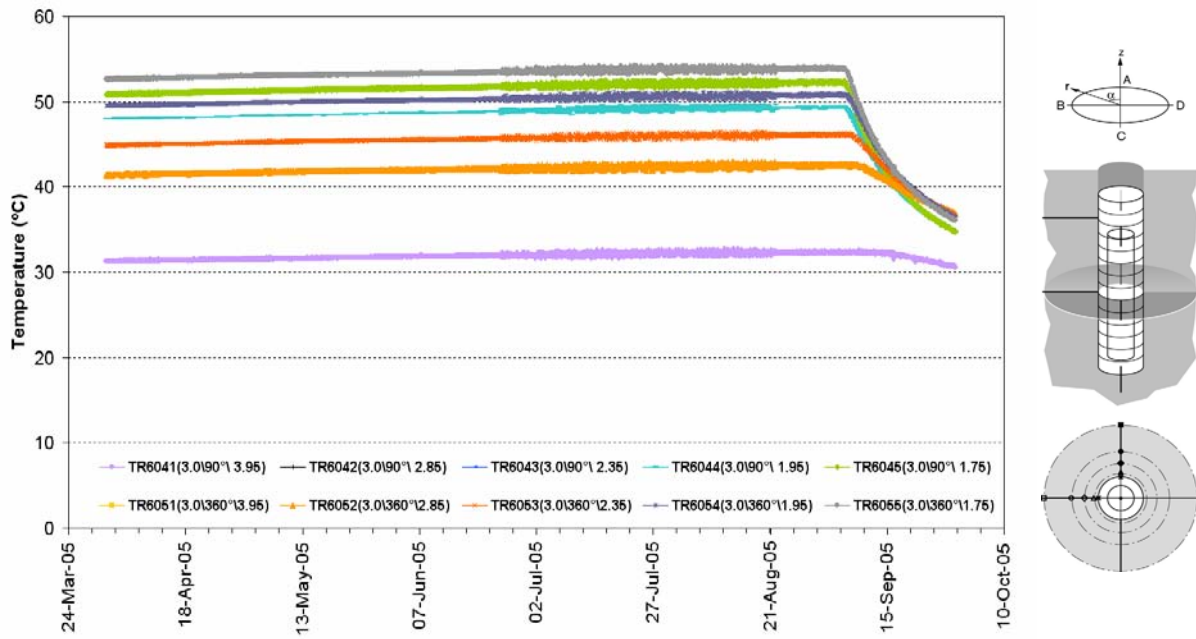
Measurements from temperature and pressure instruments located in, and around the deposition hole, provide an indication of the major environmental changes occurring during this reporting period. Figure 4-2 shows temperature change in the rock around the deposition hole. The temperature increases at a constant rate until 5<sup>th</sup> September 2005. After this date there is an exponential decrease, which is consistent with the turning off of heaters in canister 6 (deposition hole DA3435G01) [Johannesson, 2005]. The highest rate of cooling is recorded on the instruments that experienced the highest temperatures and are closest to the deposition hole (i.e. TRO45 and TRO55). By the end of the reporting period temperatures had reduced to a maximum of 36.4°C.

Figure 4-3a shows total pressure in the tunnel backfill above the deposition hole. Pressure in the deposition hole is displayed in Figure 4-3b. A trend of increasing pressure is observed up to 5<sup>th</sup> September (an increase of 1.3MPa is observed on the deepest instrument, PB623, at 4.75m) followed by a rapid decrease in pressure, particularly on instruments PB616 and PB623. This coincides with the date that drainage was opened to Section II of the Prototype Repository in which this deposition hole is situated [Johannesson, 2005]. By the end of the reporting period, decreases in pressure of 77% and 76% (from peak measurements) were recorded respectively on these two deepest instruments. An interesting observation is that for UB610, there was an initial decrease in pressure over 1 to 2 days, which then increases again after 5 days.

Velocity changes are measured between transmitter-receiver pairs on the daily ultrasonic surveys using a cross-correlation technique that allows a velocity resolution of  $\pm 2\text{m.s}^{-1}$  (see Appendix I). Figure 4-4a shows results of average P- and S-wave velocity change measured on all ray paths. Relative to previous monitoring, there is only a small change in velocity recorded during the monitoring period, with a general decrease in velocity observed when temperature and pressure starts to decrease. This will be discussed further below. There is also a minor jump in P-wave velocity of approximately  $1.3\text{m.s}^{-1}$  between the 13<sup>th</sup> and 14<sup>th</sup> September. This is not a large increase but is significant, particularly when compared to the magnitude of change that occurs on other days during the reporting period.

Further investigation of the velocity jump was undertaken to confirm that it is a real change, and not the result of an acquisition or processing artefact. Increases in P-wave velocity are systematically and consistently measured between the two days on 65 of the 80 possible raypaths, although the changes are very small, of the order  $1\text{-}2\text{m.s}^{-1}$  (the estimated uncertainty in any one measurement). The largest increase, of  $3.5\text{m.s}^{-1}$  is measured on transmitter 6 to receiver 7. Figure 4-5 shows examples plots of waveforms and cross-correlation windows from the two days. An increase in velocity on 14<sup>th</sup> September is represented by a movement of the waveform to the left. Other raypaths studied display very similar results. Significantly, not all ray paths are effected in an identical manner, nor are ray paths purely from one instrumentation borehole to another effected. Consequently this change has been interpreted as a localized change in the general rock properties rather than a systematic change in the measurement devices used in the project. There is also a small jump in average S-wave velocity on the same date, although this is much smaller than the P-wave change. 40 raypaths increase in velocity from a possible 48. The jumps coincide with a period when pressure and temperature are both decreasing. Stresses may therefore redistribute as this takes place causing a relatively sudden increase in velocities. This is further discussed below.

A variation is also observed in the amplitude measurements during the monitoring period (Figure 4-4b). There is a general trend of increasing amplitude that agrees closely with the constant rate of heating and pressure. When the peak in amplitude is achieved on 5<sup>th</sup> September 2005, P-wave had increased by 0.2dB and S-wave had increased by 0.3dB. A decrease in amplitude is then observed, which is very sensitive to the change in temperature and pressure. The decrease is more rapid than the increase recorded previously and tracks the temperature and pressure change. By the end of the reporting period, the P-wave amplitude was lower than at the start and the S-wave was slightly higher.



**Figure 4-2:** Temperature around deposition hole DA3545G01. The sensors are positioned mid-way up the deposition hole with different depths into the rock mass (see right-hand inset) [Goudarzi, 2005].

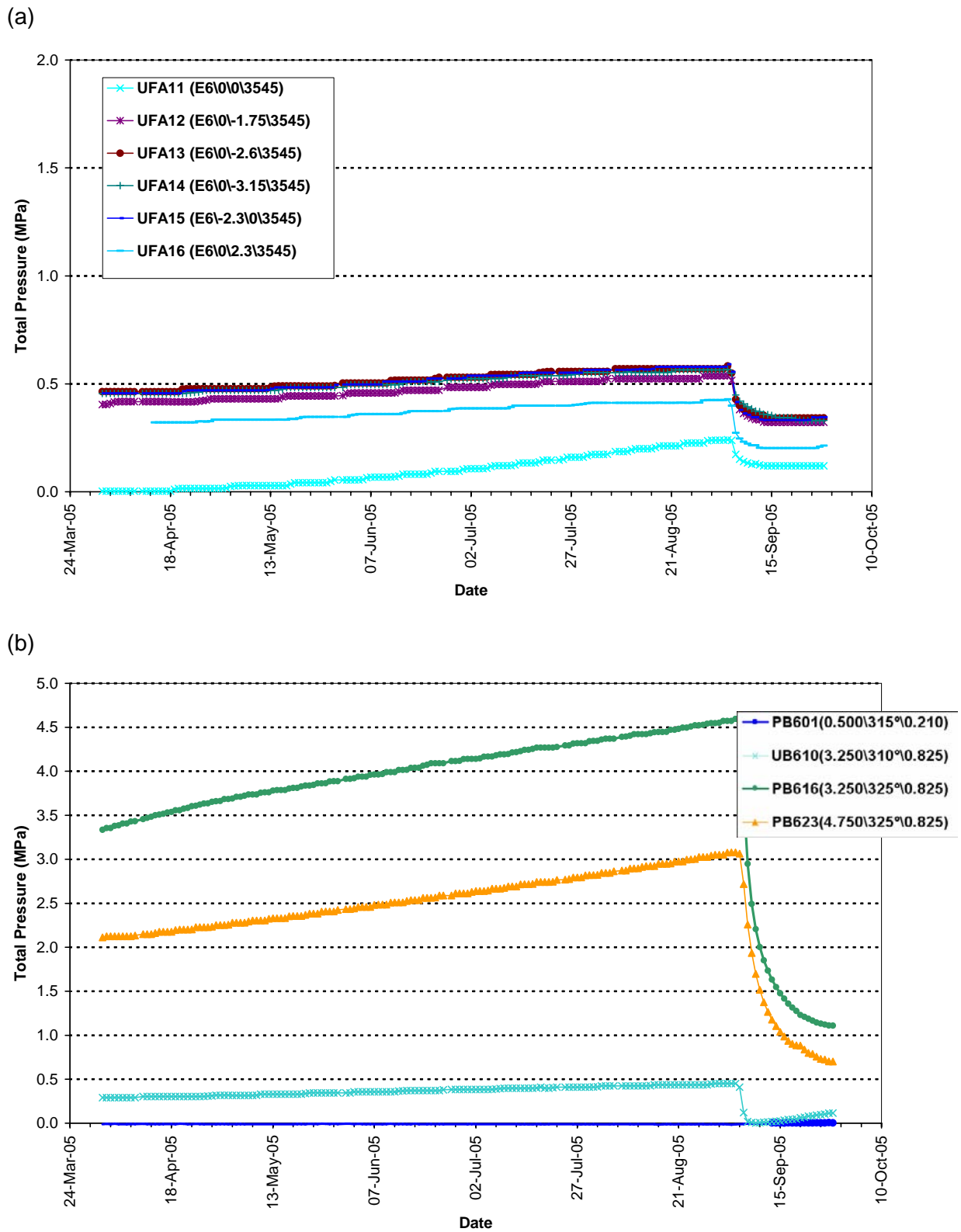


**Figure 4-3:** Total pressure in (a) the backfill over deposition hole DA3545G01; and (b) in the rock adjacent to deposition hole DA3545G01 [Goudarzi, 2005].

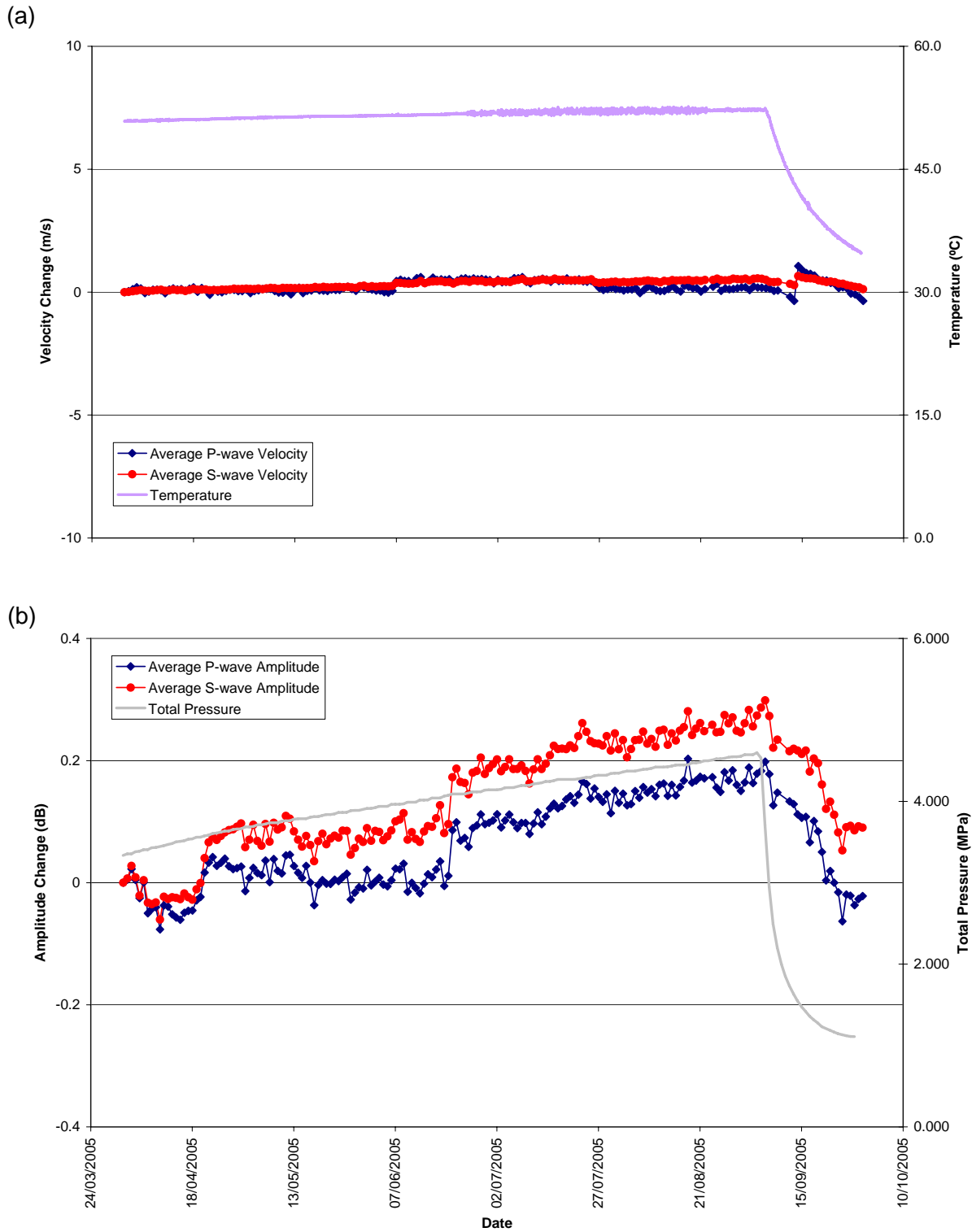


**Figure 4-4:** Average P- and S-wave (a) velocity change, and (b) amplitude change, for the reporting period. Temperature (TR6045) and total pressure (PB616) are displayed on the secondary axes.

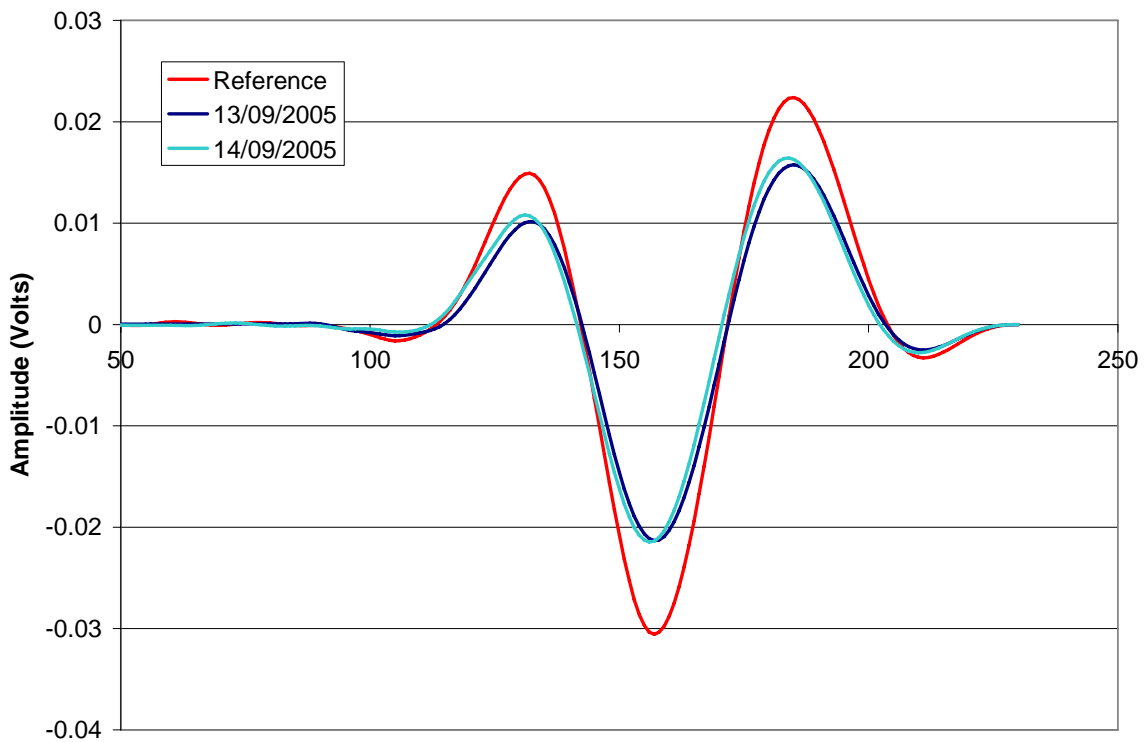
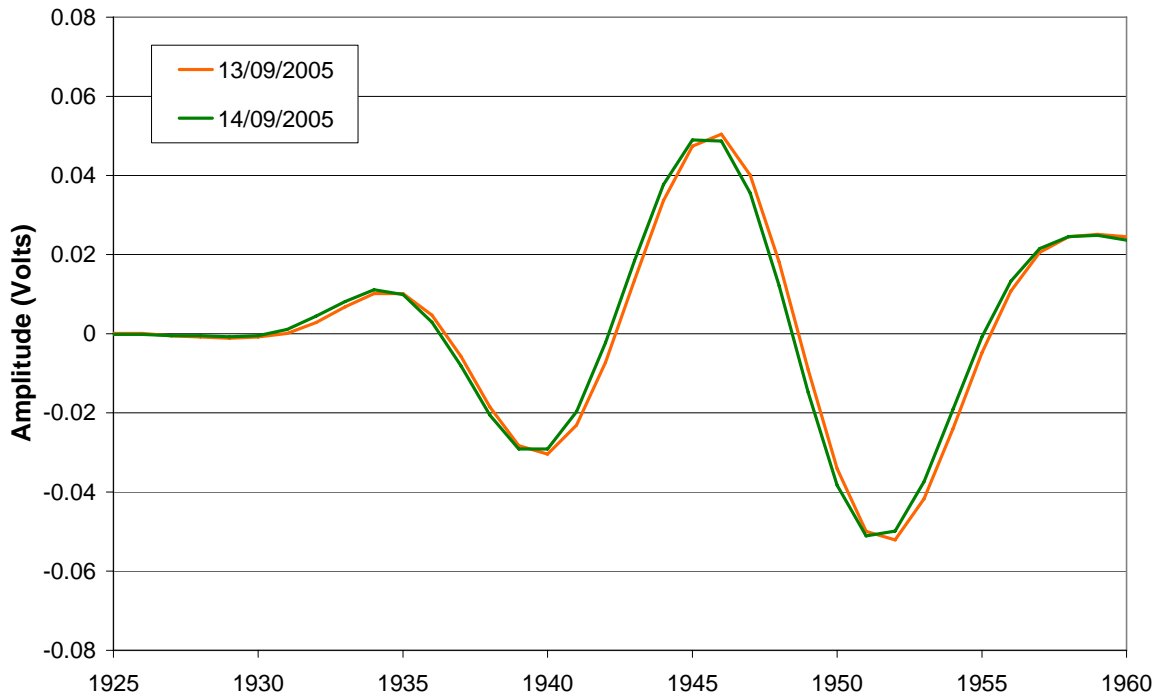


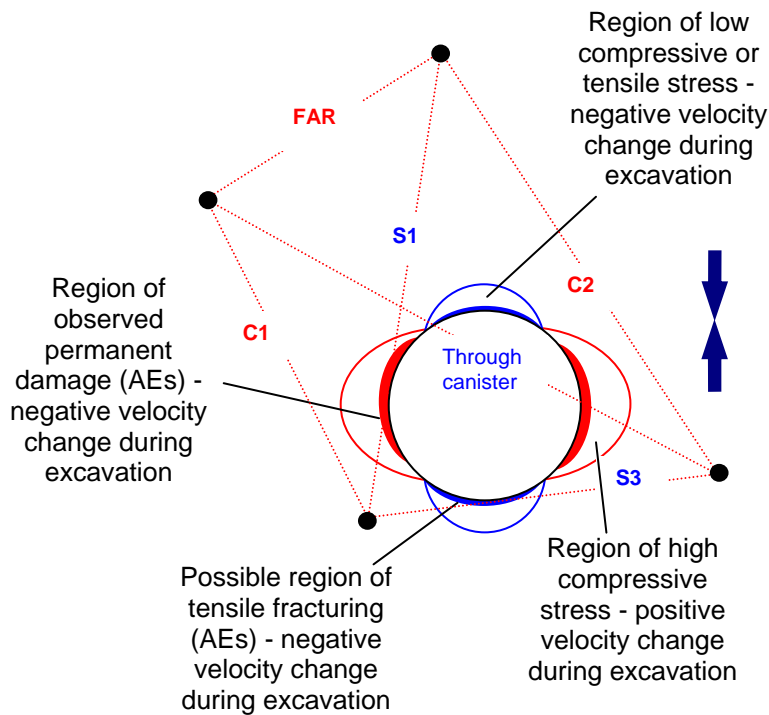
**Figure 4-5:** Example plots of (a) raw waveform data points and (b) cross correlation windows for the raypath transmitter 7 to receiver 2. The second plot also shows the reference survey from 8<sup>th</sup> December 2004.



The raypaths from the ultrasonic surveys are categorised into six types by *Pettitt et al.*[1999], depending on their orientation with respect to the deposition hole and the *in situ* stress field (Figure 4-6). An interpretation of the ultrasonic results in terms of disturbed and damaged regions around the excavation void, from the excavation phase of the experiment, is also shown in this figure. *Pettitt et al.*[2000] undertook three-dimensional elastic stress modelling to describe these zones of stress. The four plots presented in Figure 4-7 show velocity change measured on raypaths in the ‘S3’ category. These raypaths pass within centimetres of the deposition hole through the excavation damage zone, in a region of low compressive or tensile stress. Variation in velocity down the deposition hole can also be observed using these plots. The schematic diagrams to the right of the charts give a perspective of the region through which each of the raypaths pass. No significant change in P- or S-wave amplitude is observed on these raypaths until temperature and pressure in the deposition hole starts to decrease on 5<sup>th</sup> September 2005. After this date, the three raypaths passing closest to the bottom of the deposition hole experience decreases of between 5 and 12m.s<sup>-1</sup>. There is no significant change in the raypath passing closest to the tunnel at the top of the deposition hole. This raypath was also the least affected during heating [*Haycox et al.*, 2005], an occurrence that could be attributed to the rock at this depth being above the top of the canister (which is situated between 449 and 454m depth) and so does not undergo changes in temperature to the same extent as lower raypaths. Figure 4-3b shows that the largest pressure changes in the deposition hole occur deeper in the hole where the highest velocity changes are observed.

Figure 4-8 shows velocity results for raypath category ‘S1’. In this instance, raypaths pass through a region of high compressive stresses and permanent damage close to the tunnel wall imaged by relatively high AE activity during excavation. Similarly, there were a number of located events in this vicinity when heating of the canister commenced. Three of the raypaths show no significant change in velocity throughout the reporting period. The raypath that does show change, transmitter 7 to receiver 6, has a constant decrease in P-wave velocity until 5<sup>th</sup> September 2005. A more rapid decrease in P-wave velocity (and change in S-wave velocity) occurs as the rock cools. By the end of the reporting period, the P-wave velocity on this raypath has reduced by 22m.s<sup>-1</sup>. This ray path must therefore pass through a feature in the rock mass that is more sensitive to pressure or temperature changes than generally observed in this volume.

The velocity results show that significant changes during the monitoring period are generally only observed after 5<sup>th</sup> September 2005. Sixteen raypaths show a reduction of more than 4m.s<sup>-1</sup> for P-wave velocity between 5<sup>th</sup> September and the end of this reporting period. This represents a significant change of greater than 2 sample points. Three raypaths show a 4 m.s<sup>-1</sup> decrease in S-wave velocity over the same time. Transmitter 2 to receiver 6 shows the largest decrease in P-wave velocity of 18m.s<sup>-1</sup> as the rock cools and depressurises. Figure 4-9 displays these raypaths in the location visualiser of InSite relative to the location of the deposition hole. 8 raypaths on category ‘S3’ are included, 5 that pass through the deposition hole, 2 along category ‘S1’ and 1 on category ‘C1’. This result suggests that the largest decreases during cooling and depressurisation are occurring on raypaths passing through fractures adjacent to the deposition hole in a region of low compressive stress (or slightly tensile stress).



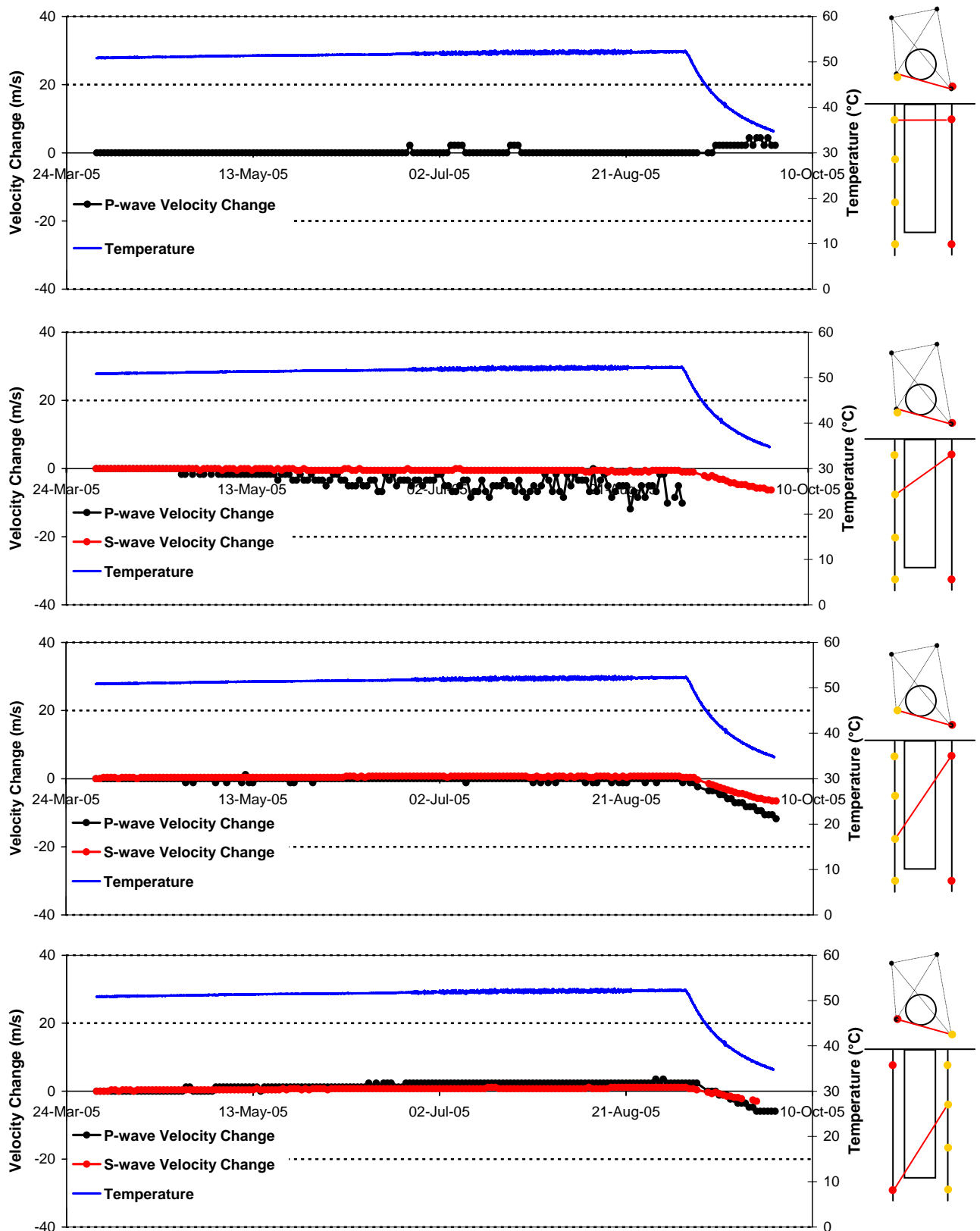
**Figure 4-6:** Interpretation of the ultrasonic results during excavation in terms of disturbed and damaged regions around the deposition hole. Zones of induced stress are inferred from elastic modelling and the  $\sigma_1$  orientation. After Pettitt et al.[1999].

Figure 4-10 and Figure 4-11 compare the results of average velocity and amplitude changes across the different raypath categories described in Figure 4-6. P-wave velocity shows a greater amount of variation than S-wave velocity. Raypaths that pass closest to the deposition hole (categories 'S1' and 'S3') exhibit the largest decreases after 5<sup>th</sup> September 2005 when temperature and pressure decrease. Other raypath categories also show small decreases but end the reporting period with a net increase in velocity due to the sudden velocity increase on 14<sup>th</sup> September as discussed earlier. For S-wave velocity, only category 'S3' that passes through a low compressive or tensile region, shows a significant difference (a decrease of more than  $2.5\text{m.s}^{-1}$ ). Category 'S1' does not experience the change in S-wave velocity that it does in P-wave velocity. This suggests a change in saturation rather than an opening of cracks and pore spaces. Overall the changes experienced are of low magnitude (not more than  $5\text{m.s}^{-1}$ ), which is small in comparison to changes of up to  $25\text{m.s}^{-1}$  that occurred during the heating phase (up to 5<sup>th</sup> September). Amplitude changes are also relatively small during this reporting period (Figure 4-11). Until 5<sup>th</sup> September P-wave amplitudes did not vary more than  $\pm 0.3\text{dB}$ . During cooling and depressurisation there is a reduction in amplitude for all categories. 'C2' experiences the largest decrease of approximately 0.7dB. S-wave amplitudes increase slightly during the first part of the reporting period followed by a decrease that follows a similar trend to the P-waves.

Figure 4-12 shows changes in Young's Modulus, Poisson's Ratio, Crack Density and Saturation parameters calculated from the average measured velocities for the ray path categories. These plots highlight the similarities between the results for raypath categories 'C1', 'C2', and 'Far'. The values remain fairly constant throughout the reporting period. Greater variation is observed on raypath categories 'S1' and 'S3'. During cooling and depressurisation there is a decrease in dynamic Young's Modulus (indicating a reduction in stiffness of the rock mass). 'S3' is affected to a greater extent, decreasing by 1.4%. 'Crack Density' and 'Saturation' of the rock mass are determined using the method of Zimmerman and King[1985], as described in Appendix 1. The 'S3'

raypath experiences an increase in crack density, whereas the others remain relatively similar during the entire period. The response of raypath 'S3' to the drop in pressure and temperature could be interpreted as the opening of existing microfractures and pore spaces in the region of tensile fracturing. Existing microcracks in this region are initially unloaded after excavation. Consequently they are more reactive to stress changes than in the compressive region where stresses act to pre-close the microcracks. As temperatures increased during the initial heating phase the thermal stresses acted to close the fractures, leading to a reduction in crack density. These fractures may now have opened again as the rock cooled and pressure from the deposition hole interior is reduced.

Figure 4-12d, shows a decrease in saturation over the reporting period for category 'S1' raypaths. This is a result of the measured decrease in P-wave velocity with only a small corresponding decrease in S-wave velocity (Figure 4-10) and is interpreted as being caused by a drying of the rock mass in the zone experiencing high compressive stresses. The step in average velocities between 13<sup>th</sup> and 14<sup>th</sup> September mentioned previously is observed here as a small but sudden change in saturation on all the ray path categories and is not so apparent in crack density. This is caused therefore by a sudden increase in fluid content of the rock mass as pressures and temperatures are removed, possibly by a shift in the conditions of the bentonite buffer within the deposition hole at this time. During the period of cooling and de-pressurisation, saturation is observed to generally decrease, possibly as a result of the combined effect of lowering fluid pressures whilst the rock remains relatively warm (>35°C).



**Figure 4-7:** Velocity changes measured on ray path category 'S3' (Figure 4-6) for deposition hole DA3545G01. Ray paths shown are from a top transmitter to receivers with increasing depth: a) transmitter,  $t_n=1$ , receiver,  $r_n=5$ ; b)  $t_n=1$ ,  $r_n=6$ ; c)  $t_n=1$ ,  $r_n=7$ ; d)  $t_n=4$ ,  $r_n=2$ . Schematic diagrams in the right margin indicate the relative locations of transmitter (red) and receiver (gold). Temperature (TR6045) is displayed on the secondary axes.

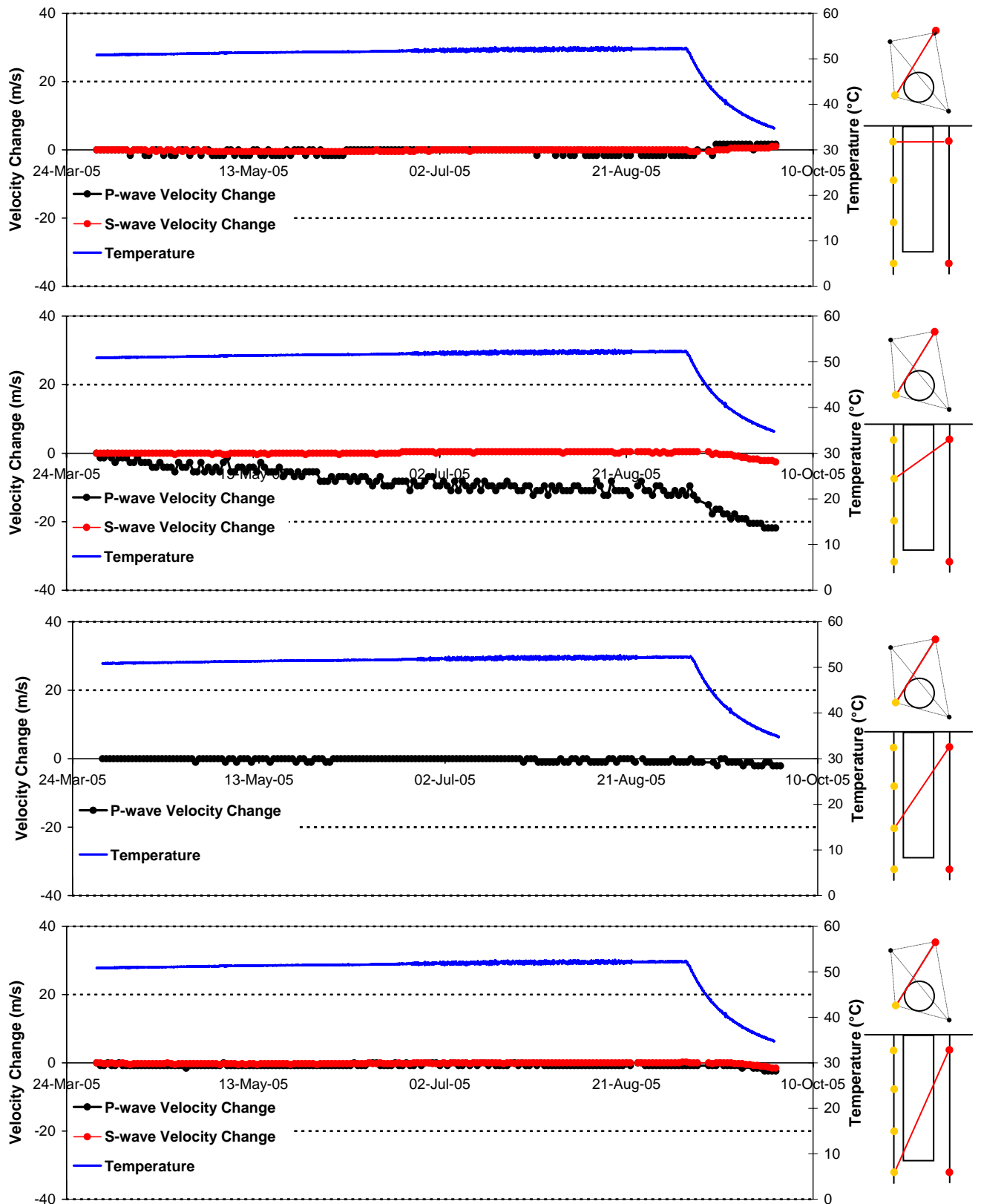


**Figure 4-8:** Velocity changes measured on ray path category 'S1' (Figure 4-6) for deposition hole DA3545G01. Ray paths shown are from a top transmitter to receivers with increasing depth: a) transmitter,  $t_n=7$ , receiver,  $r_n=5$ ; b)  $t_n=7$ ,  $r_n=6$ ; c)  $t_n=7$ ,  $r_n=7$ ; d)  $t_n=7$ ,  $r_n=8$ . Schematic diagrams in the right margin indicate the relative locations of transmitter (red) and receiver (gold). Temperature (TR6045) is displayed on the secondary axes.

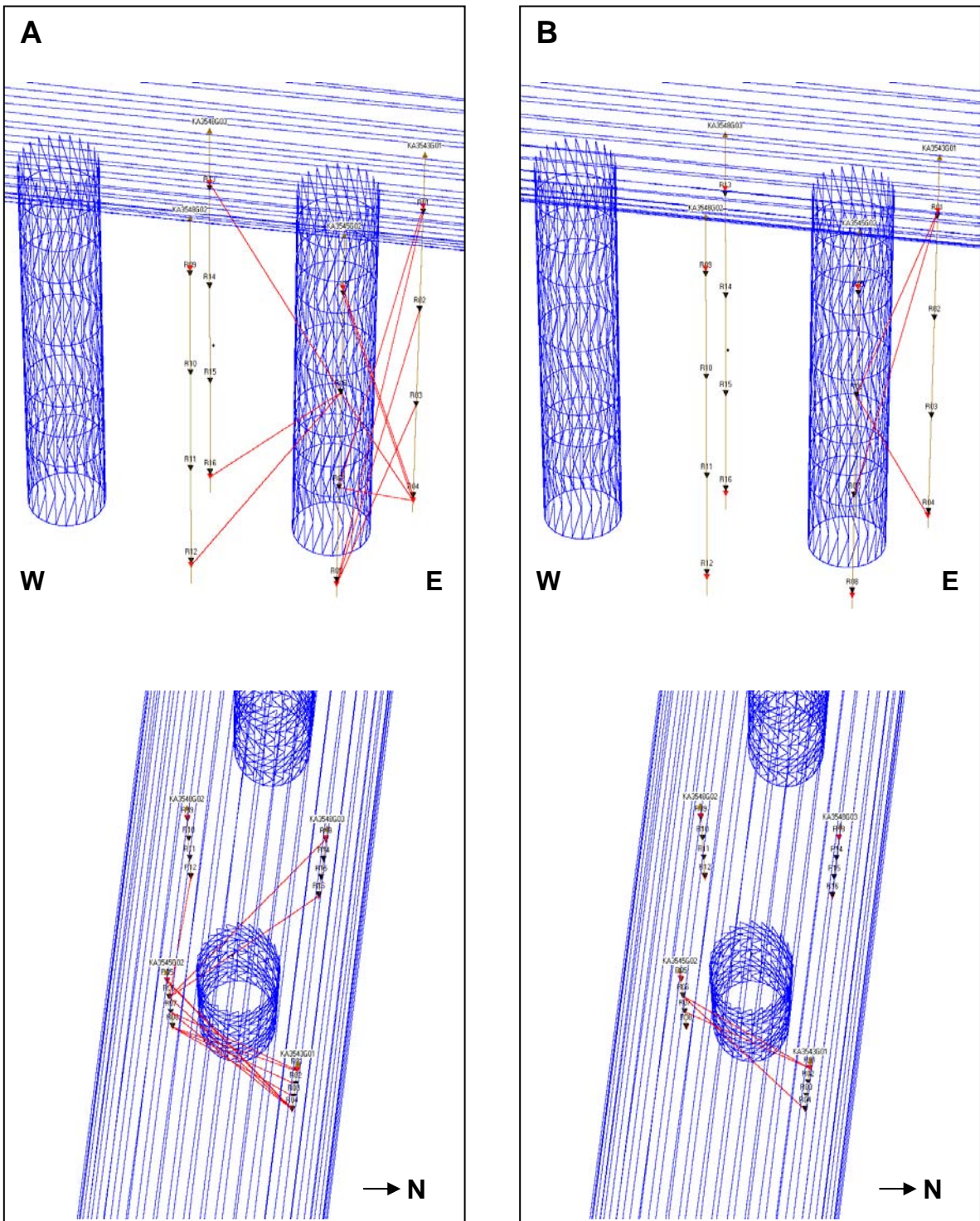


**Figure 4-9:** Raypaths showing a significant decrease (greater than  $4\text{m}\cdot\text{s}^{-1}$ ) after 5<sup>th</sup> September 2005 for A) P-wave velocity and B) S-wave velocity. The upper plots are viewed northwards, the lower plots are viewed just off the vertical.

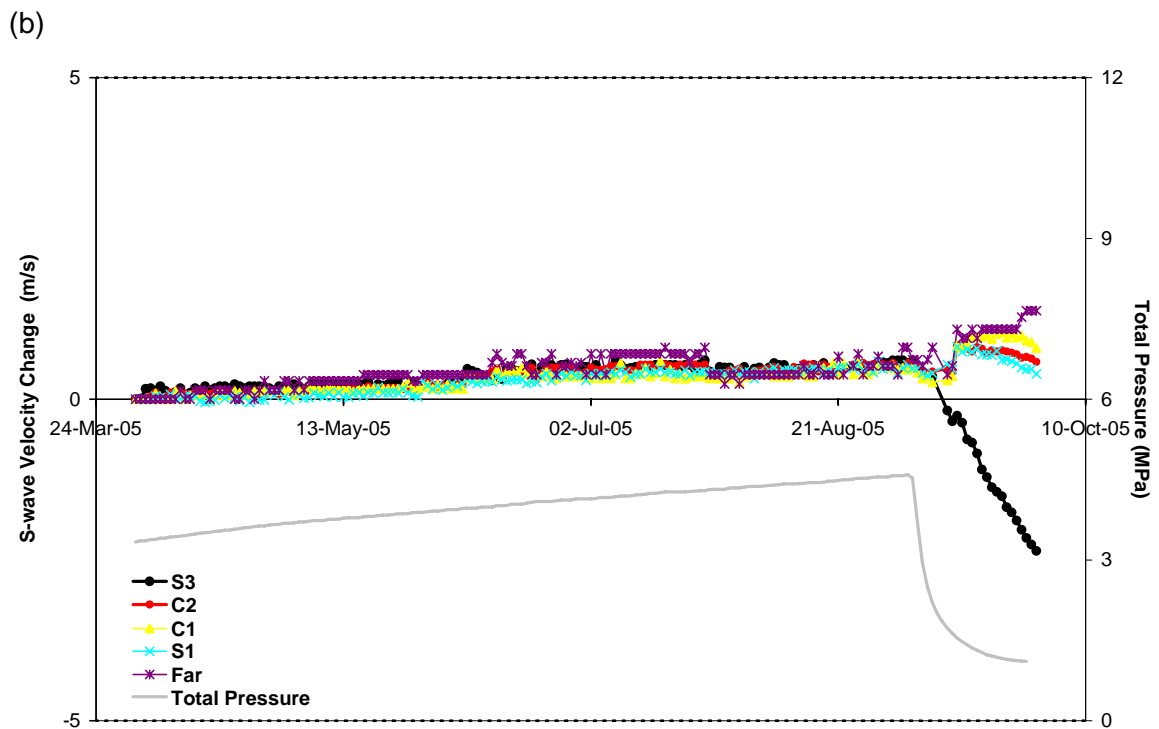
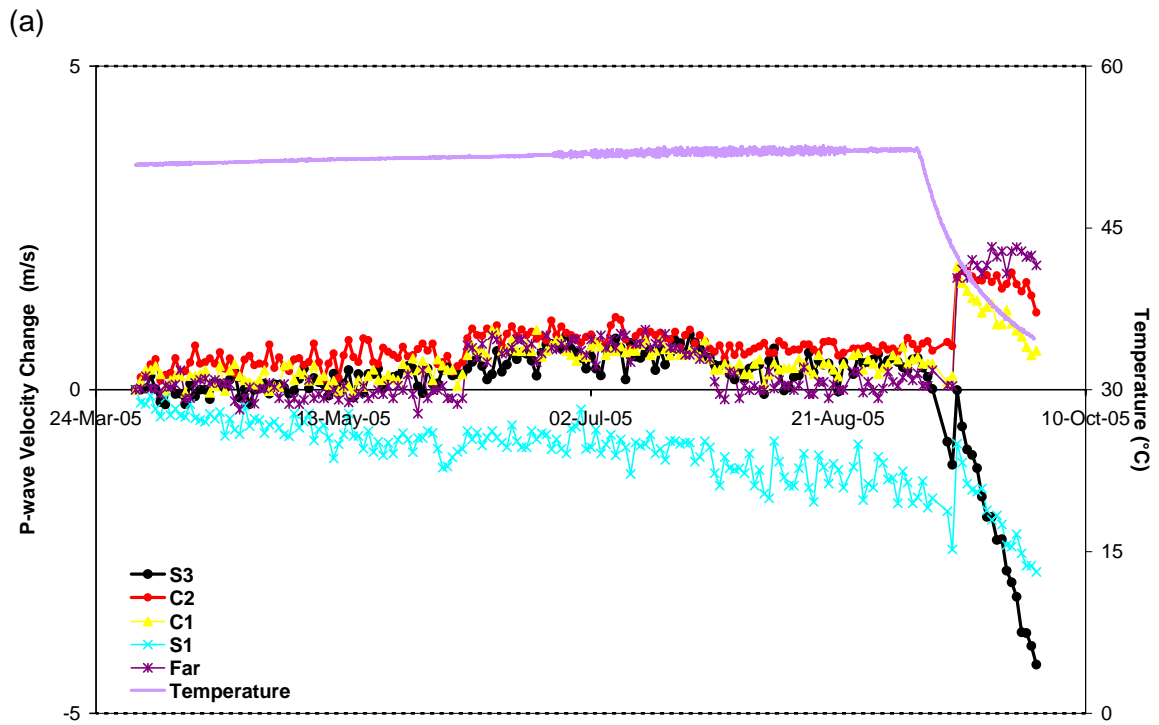


**Figure 4-10:** Velocity change plots of 5 raypath categories around deposition hole DA3545G01 for (a) P-waves and (b) S-waves. Temperature (TR6045) and total pressure (PB616) are displayed on the secondary axes.

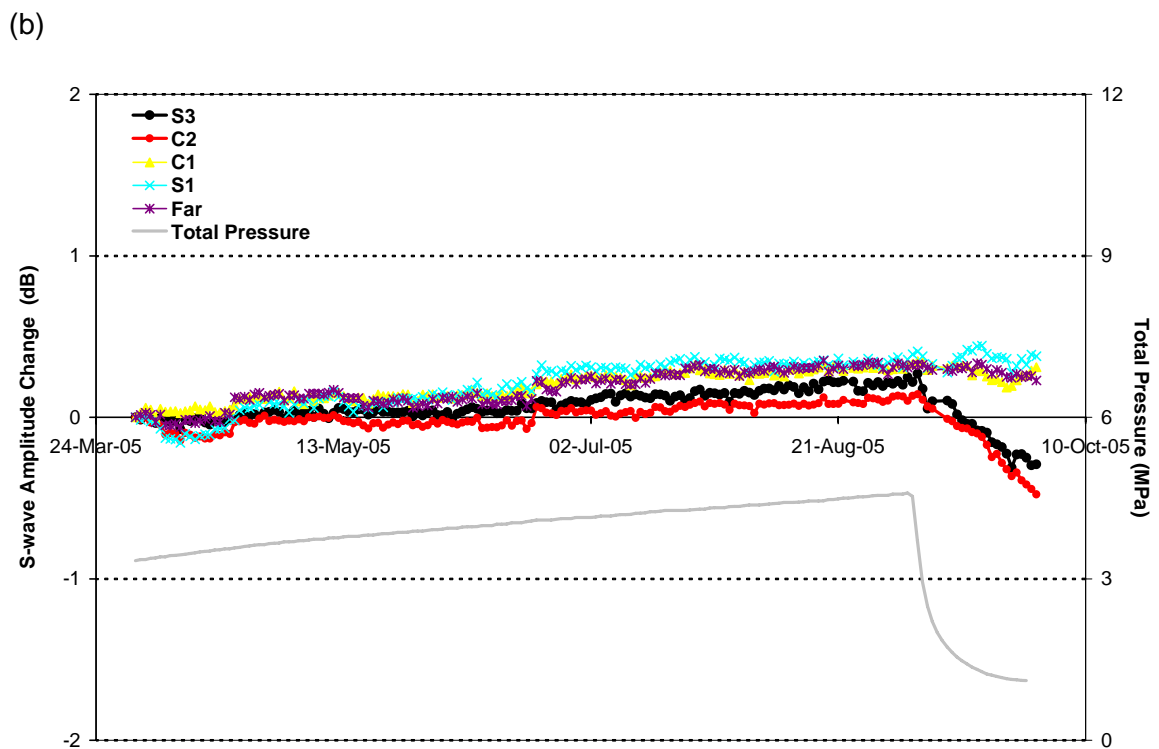
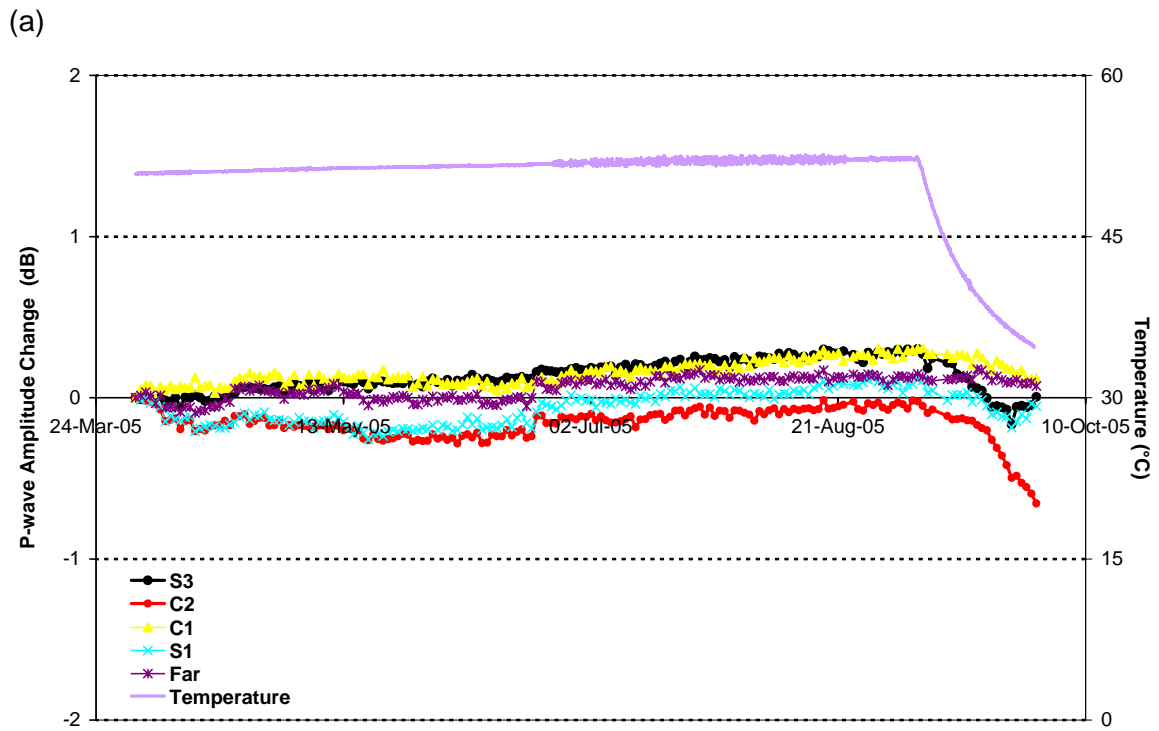


**Figure 4-11:** Amplitude change plots of 5 raypath categories around deposition hole DA3545G01 for (a) P-waves and (b) S-waves. Temperature (TR6045) and total pressure (PB616) are displayed on the secondary axes.



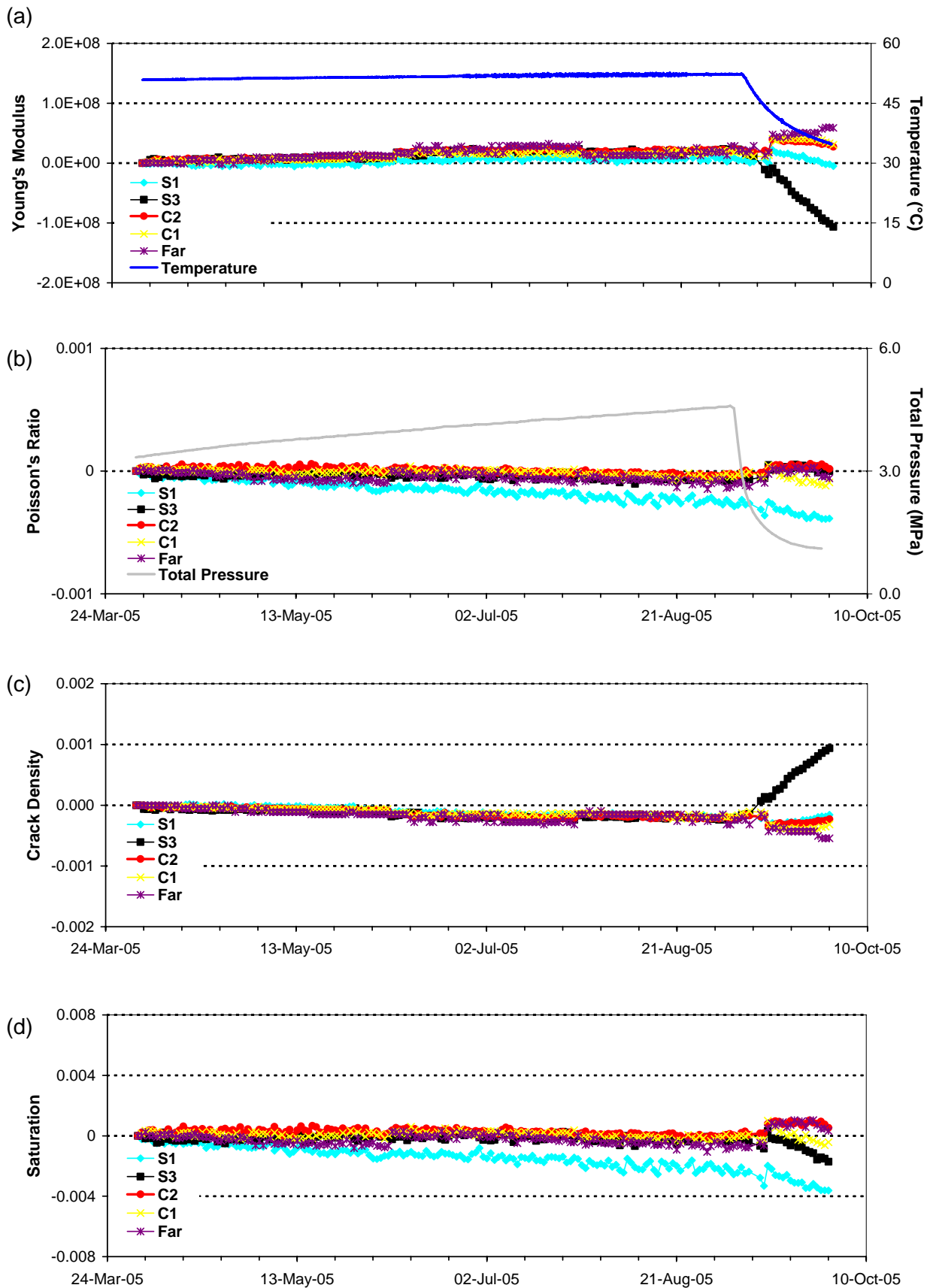


**Figure 4-12:** Modulus during this reporting period for average *P*- and *S*-wave velocity values on different raypath orientations. (a) Young's Modulus, (b) Poisson's Ratio, (c) Crack Density and (d) Saturation. Raypath orientations are described in Figure 4-6. Temperature (TR6045) and total pressure (PB616) are displayed on the secondary axes.

## 4.2 Acoustic Emissions

Acoustic emissions have been processed following the procedures outlined in Appendix I. 38 events have been located with high confidence from 82 triggered events recorded during this period (46% located events from triggers). Estimated uncertainties on these events are of the order 10cm as described by calibration ‘hits’ performed within the deposition hole.

The temporal response of the triggers and located events are shown in Figure 4-13. A trigger is described as an event that has been acquired by the system, but is not of sufficient quality to be located during the processing procedure. ‘Noise’ events, produced from either electrical or man-made sources, have been removed from this count because they are not determined to be ‘real’ events. Figure 4-13 a shows the temporal distribution of AE triggers. The largest number of triggers occurs on 24<sup>th</sup> May 2005. On the cumulative plot this appears as a large jump, with 18% of all triggers during this reporting period happening on this day. Otherwise, the number of triggers per day is between 1 and 3 recorded sporadically throughout the period. The rate of activity increases slightly in early September, marked by a change in slope on the cumulative plots, and co-incident with the pressure and temperature decreases. In terms of located events, shown in Figure 4-13b, relatively few have been obtained during this 6-month period when compared to the excavation period [Pettitt *et al.*, 1999]. The rate of activity is slightly lower during this period (0.21 Events per day on average) compared to the previous six months of heating (0.32 Events per day on average after omitting the large pressure drop observed in that time period). A maximum of 2 events per day occur on 24<sup>th</sup> April and 13<sup>th</sup> September. Interestingly, only one event was located on the 24<sup>th</sup> May from 15 triggers. Examination of the waveforms for these events shows them to be lower frequency than that generally observed and located in the sidewall of the tunnel (outside the monitored volume around deposition hole DA3545G01). These events are possibly associated with an instrumentation borehole.

Figure 4-14 shows the spatial distribution of located AEs. Three projections are presented, which show the events in relation to the deposition holes and tunnel. The majority of the events locate in the immediate vicinity of deposition hole DA3545G01. Two events also locate close to the neighbouring deposition hole DA3551G01. Waveforms of selected events are shown in Figure 4-15 to demonstrate the high quality data collected. A cluster of events, indicated as point i in Figure 4-14, is situated on the north-east side of deposition hole DA3545G01, at a depth of 457.2m just above the depth of the deposition-hole floor. Nine events of varying magnitude make up the cluster. The events may be located closer to the deposition-hole wall than the locations suggest due to larger uncertainties caused by ray paths passing around the deposition hole void to the receivers. Another cluster of events are observed on deposition hole DA3545G01 at a depth of approximately 451.5m.

In previous monitoring periods, the majority of events were distributed in the NE and SW quadrants which coincide with regions of increased compressive stress as imaged during excavation and initial stages of heating [Pettitt *et al.*, 2000; Pettitt *et al.*, 2002; Haycox *et al.*, 2005]. Smaller clusters were observed in orthogonal regions of low-compressive or tensile stress. Figure 4-16 compares plan views of the activity during excavation and this reporting period. The events observed here are consistent with these previous results with the small amount of clustering locating in regions of previous activity. The events are therefore interpreted as a continuation of activity in the previously imaged damage zone and, similar to during excavation and initial heating, are created either by movement on pre-existing microcracks, or as a result of extension or formation of new microcracks in the existing damaged region.

Four events are located in the rock mass between the two deposition holes between 455.3 and 455.7m depth. The events are believed to coincide with a semi-horizontal macroscopic fracture that is observed to intersect the deposition holes at this height [Pettitt *et al.*, 2000]. Three low-magnitude events were also observed along this fracture during the excavation phase [Pettitt *et al.*, 1999] and 11 events were located during early stages of heating [Haycox *et al.*, 2005].

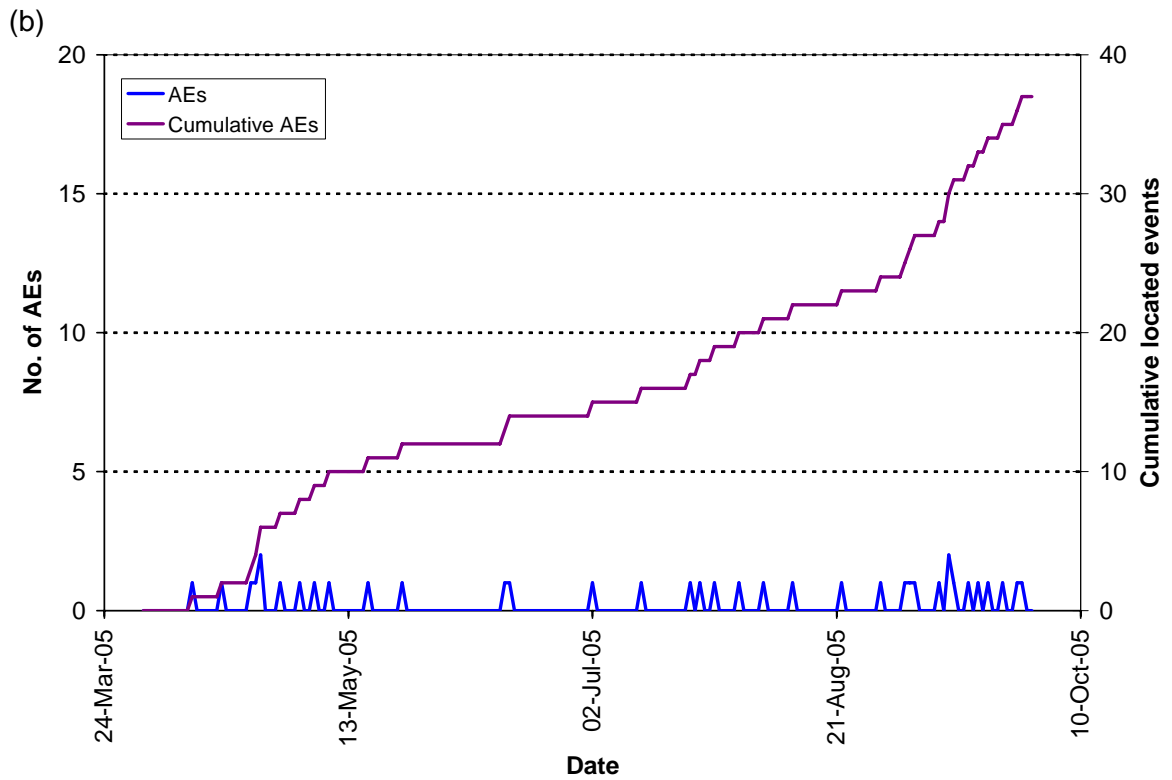
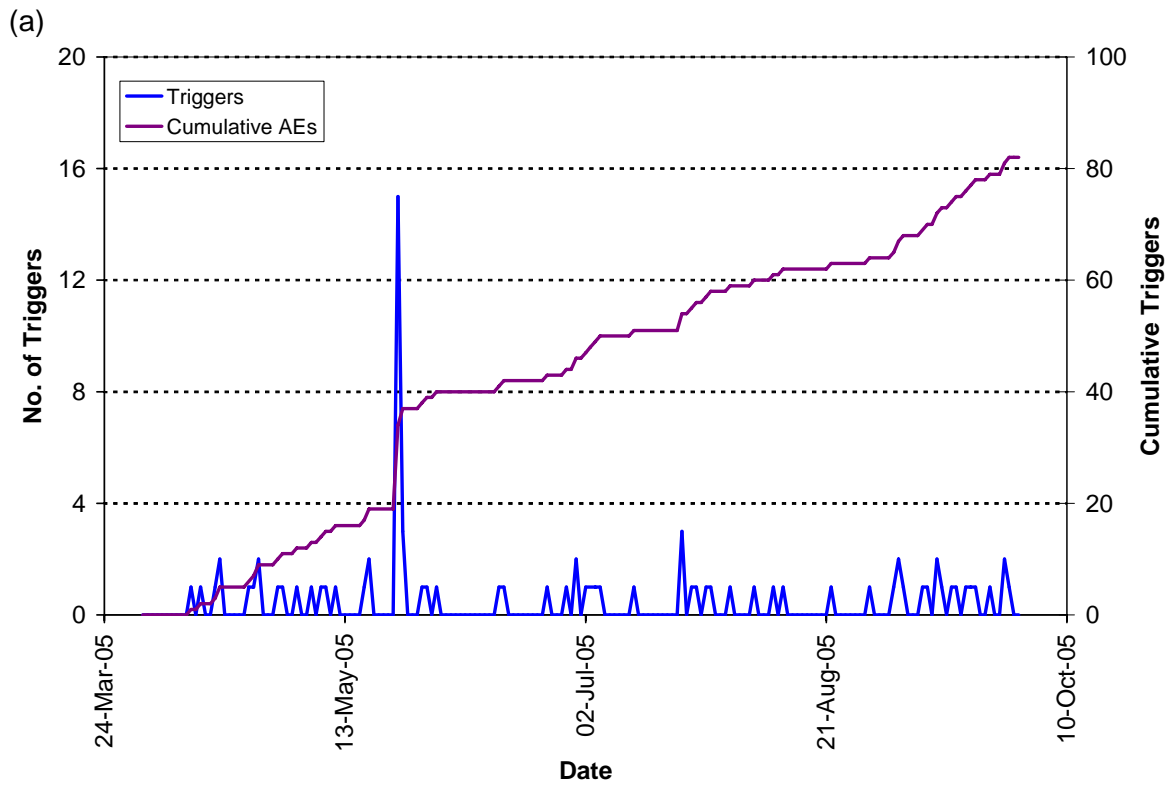


**Figure 4-13:** Temporal response plot of (a) AE triggers and (b) located AEs; number per day on left axes and cumulative number right hand axes.

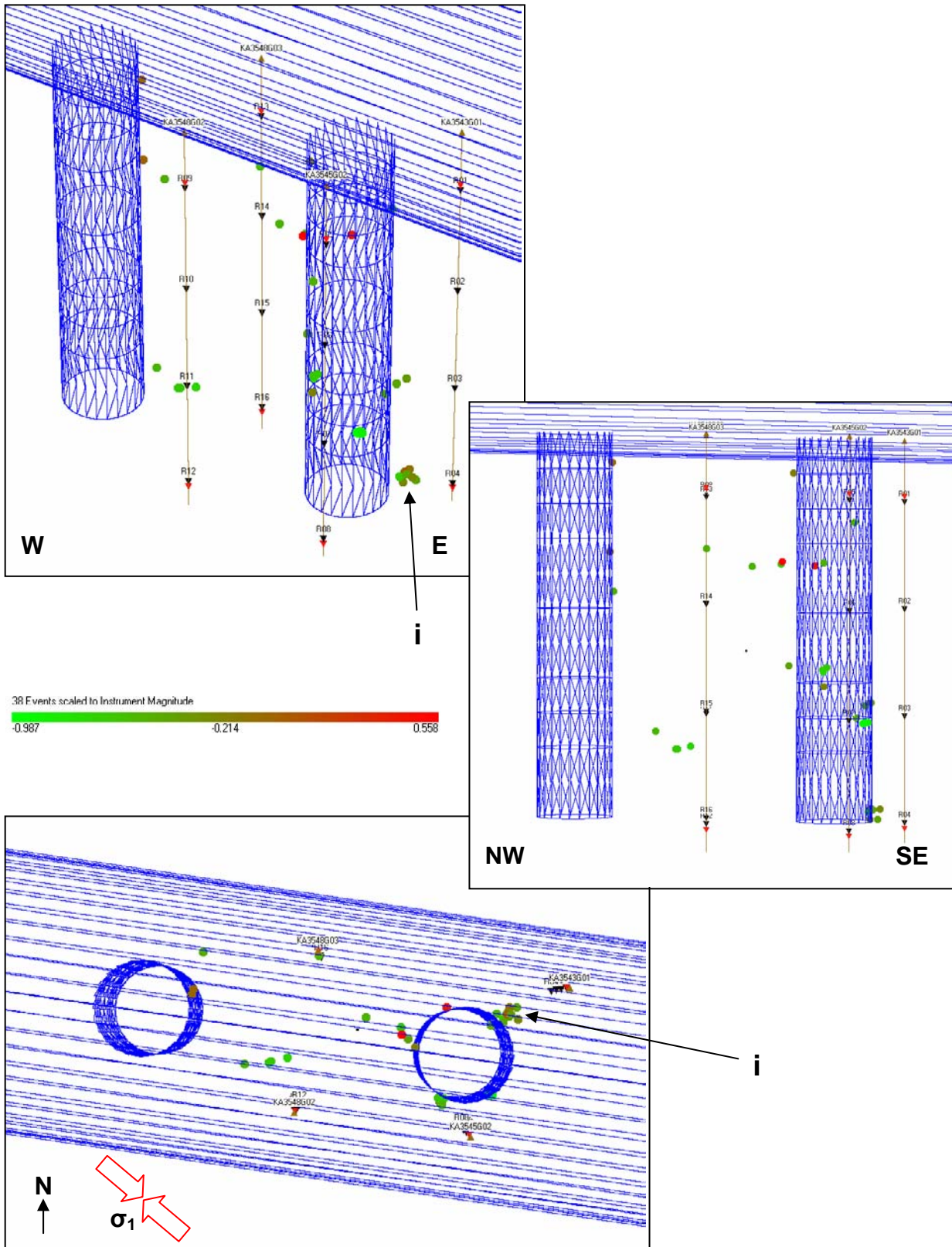


**Figure 4-14:** Three views of AE activity located around deposition holes DA3545G01 and DA3551G01. (Top: Oblique view looking North. Middle: Transverse view looking north. Bottom: Plan view). A cluster, further discussed in the text, is marked *i*.

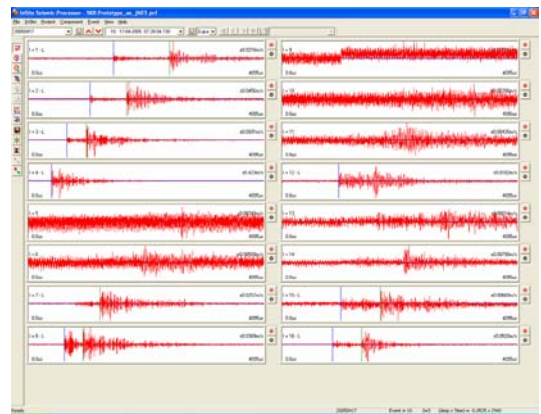
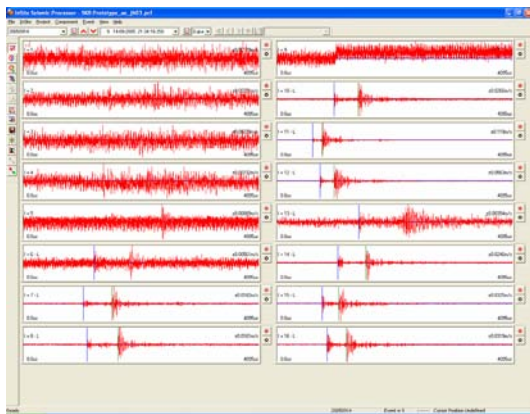
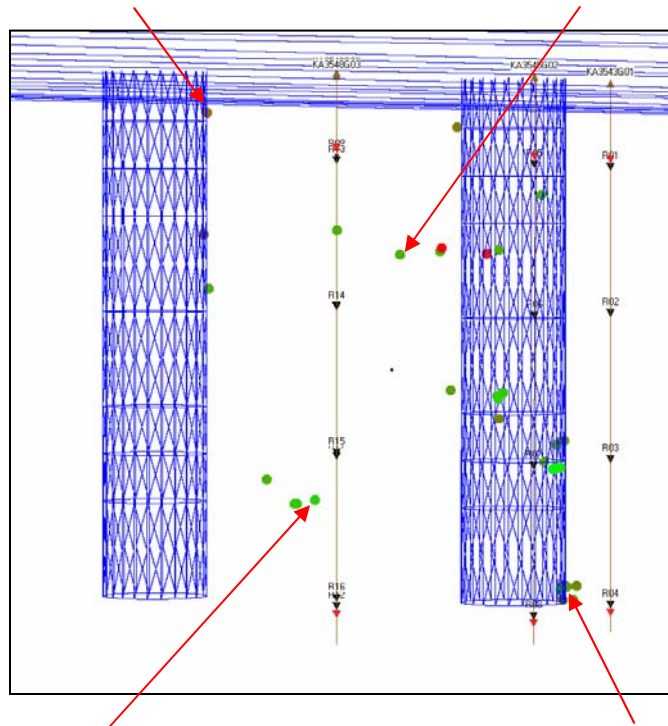
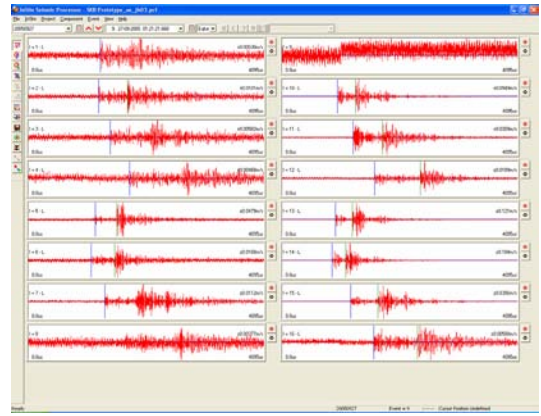
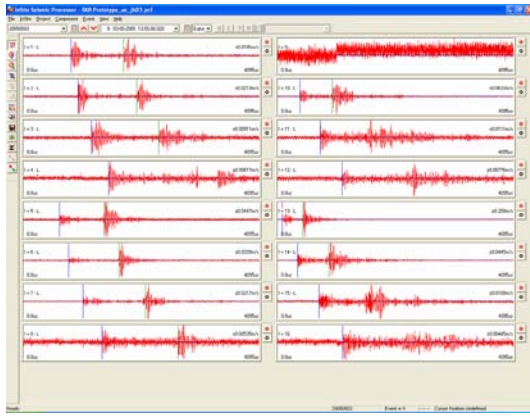


**Figure 4-15:** Waveforms from selected events shown in relation to a transverse view of AE activity.

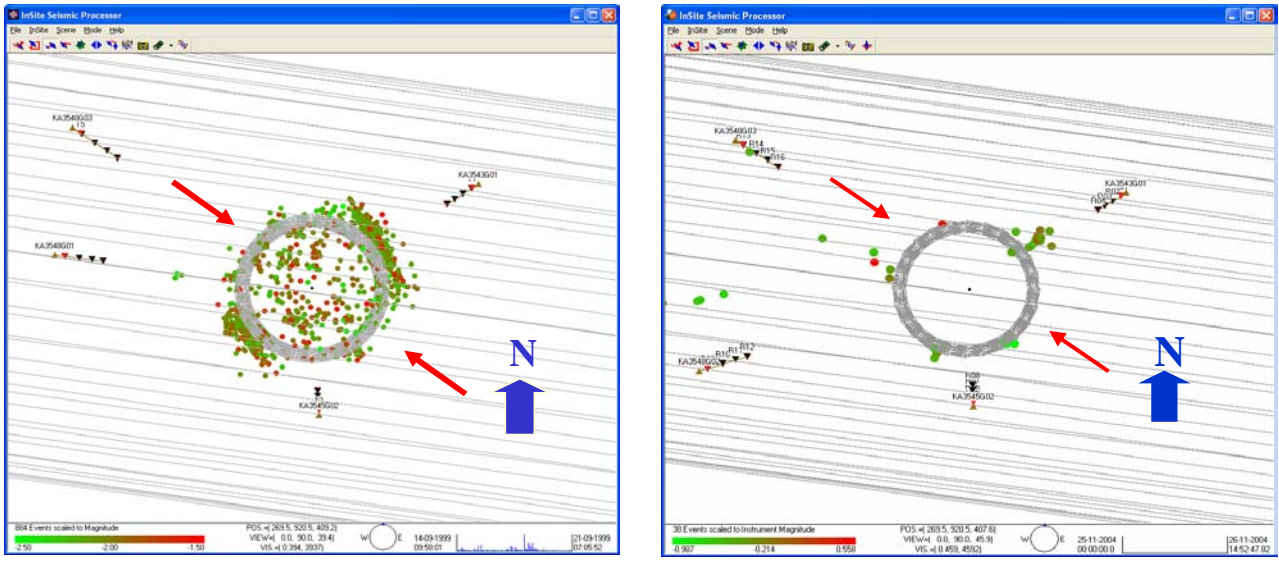


*Figure 4-16: Plan view of AEs located around deposition hole DA3545G01 during (a) the excavation phase, and (b) this reporting period. The red arrows mark the orientation of the principle stress.*





## 5 Summary of Monitoring to Date

This section of the report investigates how the results obtained during the reporting period relate to observations from previous monitoring in the Prototype Repository since the start of heating and pressurisation in March 2003.

Figure 5-1a shows average P- and S-wave velocity change and Figure 5-1b shows average amplitude change through the entire monitoring period. Also plotted on the graphs are temperature and pressure measurements from the rock adjacent to deposition hole DA3435G01. Throughout the monitoring there have been three main phases of changing environmental conditions, summarised in Table 5-1. In the first phase, temperature rose rapidly in the first few months of monitoring after the heaters in the canister were switched on. In the second phase, pressure rose rapidly after drainage from the tunnel was closed. This resulted in damage to the canister and the heaters being temporarily switched off. The third phase began in September 2005, close to the end of the latest monitoring period, when drainage was opened and the heaters switched off again, resulting in a cooling and de-pressurisation of the deposition hole.

Table 5-1 also summarises the AE and ultrasonic observations from the different phases. It will be shown in discussions below that these changes are complicated by the three-dimensional stress state of the rock around the deposition hole, and by the coupled nature of the pressure and temperature effects. At the start of heating, when temperatures rose rapidly, average P and S-wave velocities initially dropped and then began to steadily increase. In the second two phases a greater reduction in temperature occurred in September 2005 than in December 2004. In December 2004, there were significant increases in P- and S-wave velocities and amplitudes; a result that is opposite to what would be expected. This does not occur in September 2005, in which minor decreases in velocities and amplitudes have so far been observed. The difference between these two phases is that in December 2004 pressure also increased rapidly from a background level, and in September 2005 pressure decreased from a high level (although remaining relatively high, >1MPa). This observation suggests that rapid temperature change is not the most important influence on changes in measured velocity and amplitude (and consequently properties of the rock) during these times of rapid cooling and whilst pressures from the deposition-hole interior are high.

Pressure from within the deposition hole, caused by hydraulic pressure and swelling of the bentonite buffer, is the primary constraint on changes to properties of the rock around the deposition hole since 1<sup>st</sup> November 2004 when drainage was closed. The drainage closure led to an increase in total pressure in the tunnel [Haycox *et al.*, 2005]. Changes in velocity and amplitude on raypaths nearest the tunnel were observed on 26<sup>th</sup> November 2004. It was not until 5<sup>th</sup> December, when an 'event' inside the deposition hole suddenly allowed a transfer of pressure from the tunnel, that an increase in total pressure was measured inside the deposition hole. Thereafter, pressure in the deposition hole continued to increase despite constant pressures in the tunnel. The drainage was opened again on 5<sup>th</sup> September 2005, causing a rapid reduction in pressure in the deposition hole.

Average velocity and modulus changes for the five raypath categories, described in the previous section, are presented in Figure 5-2 to Figure 5-6. These changes are summarised in Table 5-1 and in schematic diagrams for each of the phases in Figure 5-9, Figure 5-10, and Figure 5-11.

A detailed description of the response of the rock to heating in Phase 1 is presented by *Haycox et al.*, [2005]. All raypath categories show an overall increase in velocity over the heating period, albeit with different temporal responses. 'S3' raypaths passing through the low compressive or tensile region show the largest overall increase in velocity ( $25\text{m}\cdot\text{s}^{-1}$  for P-wave and  $10\text{m}\cdot\text{s}^{-1}$  for S-wave). Raypath categories passing through the compressive zone exhibit less average increase (categories 'S1', 'C1', 'C2'). The 'S3' category passes through a volume that is unloaded and hence experiences low compressive stresses. This volume responds more rapidly to thermal stresses because existing microfractures are initially unloaded and hence more open than microfractures in the compressive region. The compressive stresses will be variable to orientation which may explain small differences between individual raypaths.

In the first few months of heating, another effect is superimposed onto the rock's response to thermal stresses. This is measured as a reduction in P-wave velocities compared to S-wave velocities in the first few months of heating. A desaturation occurs on all raypath categories, other than 'S3'. This must be caused by a drying of the rock mass, in the zones experiencing high compressive stresses, as heat is applied to the rock (i.e. both temperature and pressure are acting to expel moisture). In the low-compressed, or tensile, region saturation increases during this period. This is probably caused by hot fluids expanding into the open microfracture fabric.

In Phase 2, November and December 2004, all raypath categories show an increase in velocity when pressure increases, although the extent of the velocity increase varies. For instance in terms of P-wave velocity, 'C2' only exhibits a change of  $0.9\text{m}\cdot\text{s}^{-1}$ , while 'S1' increases by approximately  $5.5\text{m}\cdot\text{s}^{-1}$  over 5 days. The pressure increase can be interpreted as increasing the stiffness of the rock with a corresponding decrease in crack density. The magnitude increase is greater for 'S1' and 'S3' categories because the volumes through which they pass are close to the deposition holes and contain a higher proportion of microfractures in an excavation damage zone. The pressure increase acts as a confining pressure on the rock mass leading to a closure of the pre-existing microcrack fabric and so a reduction in crack density. We observe that only a relatively small pressure increase is sufficient to close this microcrack fabric in the volumes already under high compressive stresses, leading to an initially high rate of change in measured velocities followed by a constant level, even though pressures may keep increasing afterwards. From Figure 5-2 the required pressure increase is approximately 1.5MPa.

Another effect at this time is a rapid cooling of the rock when the heater inside the canister is switched off (for 13 days between 2<sup>nd</sup> and 15<sup>th</sup> December 2004), followed by warming as the rock is reheated. The majority of categories do not show a significant change in P- or S-wave velocity during this period. However, category 'S3' exhibits a decrease in P- and S-wave velocity followed by an increase that mirrors the rate at which temperature changes (Figure 5-3). This category was found to be the most sensitive to thermal stresses during the initial stages of heating. When the rock cools, thermal stresses acting in this volume of low compressive (or slightly tensile) stresses reduce causing unloading of the microcracks. Microcracks close again when the rock is reheated and thermal stresses increase.

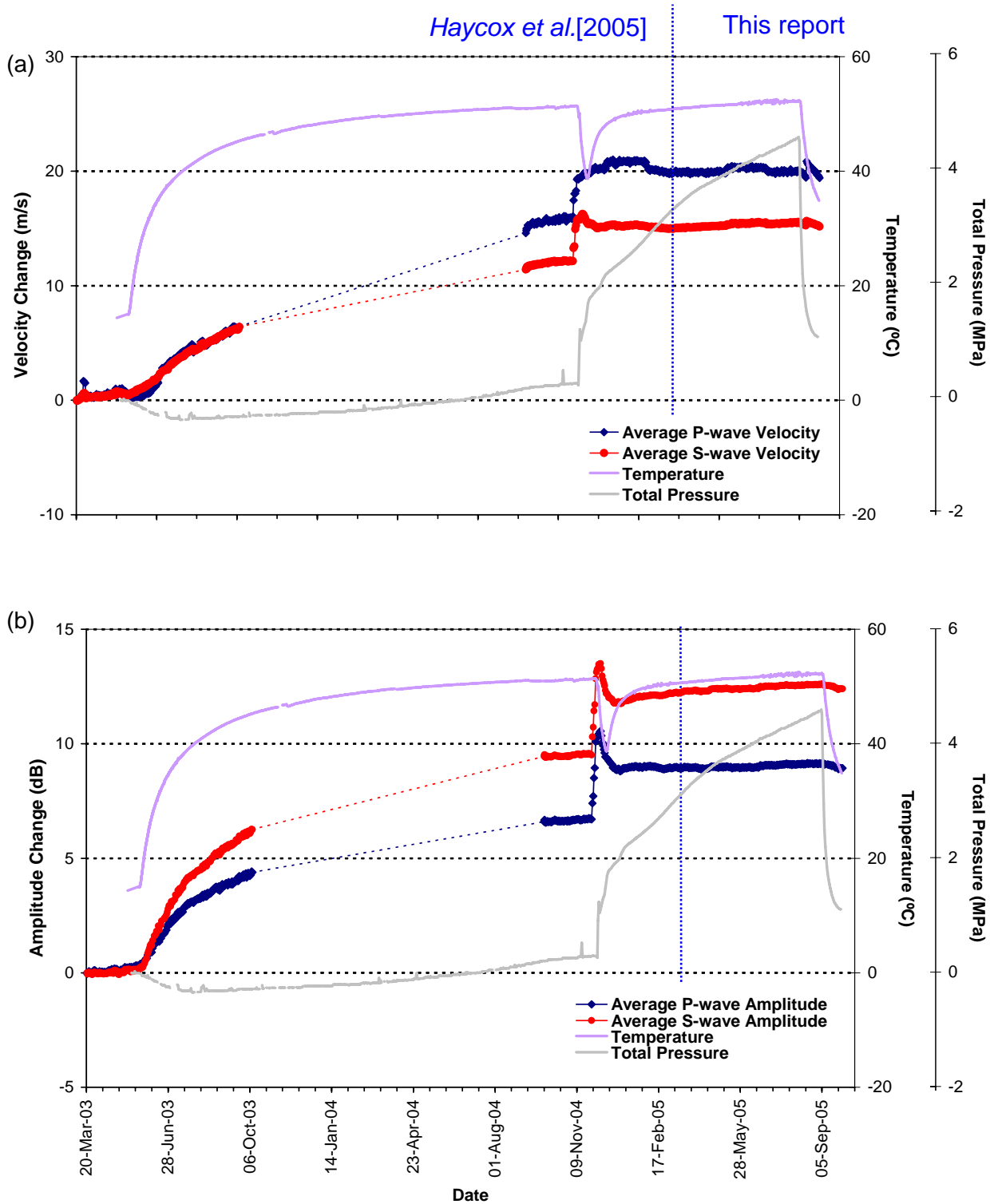
In September 2005, pressure and temperature reduce concurrently. This change is more extensively discussed in Section 4.1 of this report. Although temperature and pressure changes are significant, the change in velocity is generally very low. An exception to this is category 'S3'. A decrease of  $4.3\text{m}\cdot\text{s}^{-1}$  and  $2.9\text{m}\cdot\text{s}^{-1}$  are measured over this time for P- and S-wave velocity respectively. This category is observed as the most sensitive to changes in temperature during the previous two changes. As temperature decreases, thermal stresses again reduce in this volume causing microcracks to reopen and resulting in an increase in crack density and reduced stiffness of the rock.

In both Phase 2 and Phase 3 very little change, associated with temperature change, is observed on the other raypath categories, indicating they are relatively insensitive to thermal stresses. During the initial heating period the velocity measurements for raypath category 'S1', passing through the volume of high compressive stresses, were shown to be relatively insensitive to heating even without a confining pressure. It would seem logical that with a confining pressure of 1MPa, and much of the pre-existing microcrack fabric being further closed, the measurements would be more insensitive to thermal stresses.

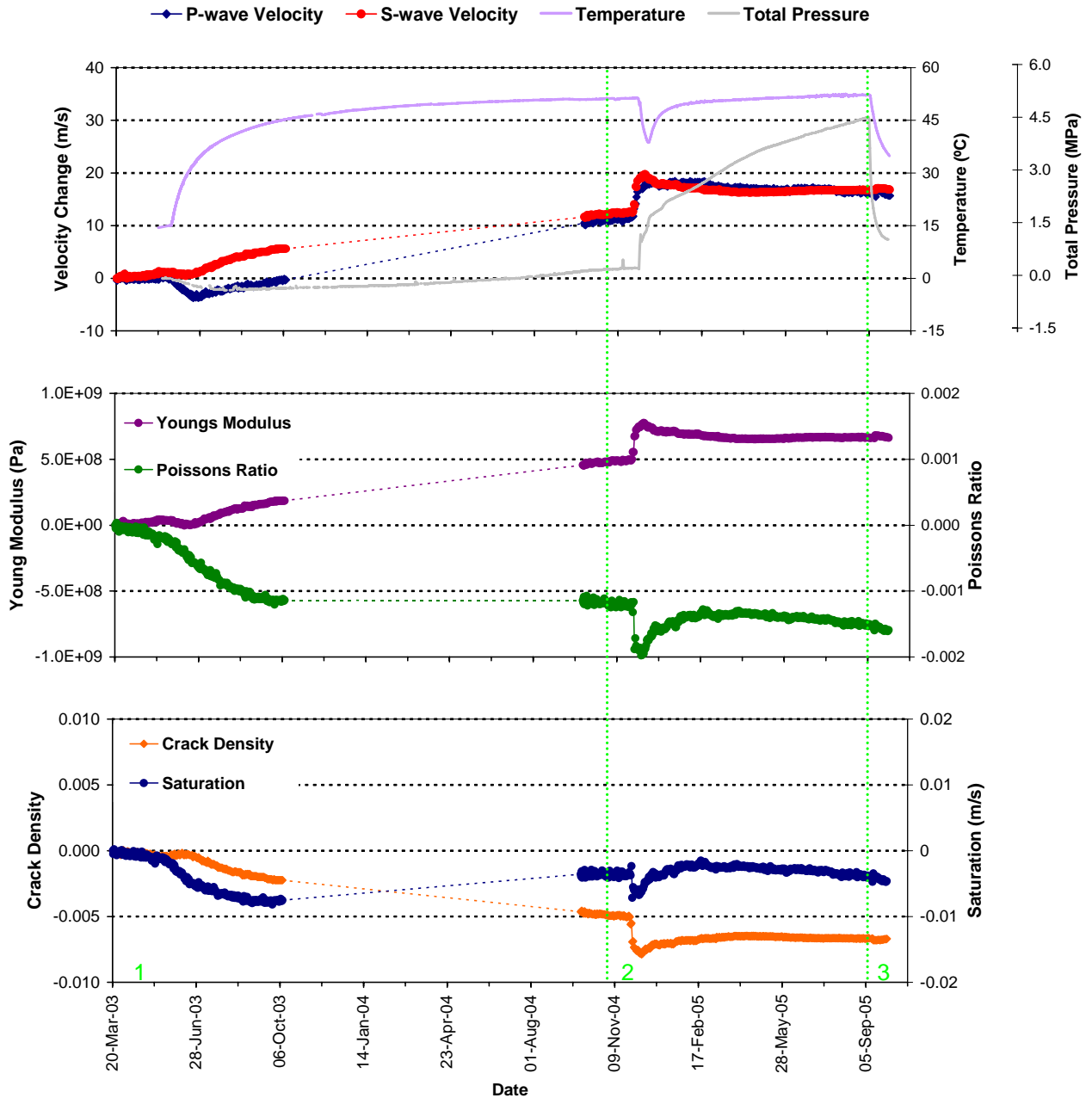
Raypaths passing through the deposition hole have not been used in this analysis of the rock mass as they are likely to have complicated travel paths associated with the deposition hole geometry, canister and bentonite buffer, and rock-fluid-bentonite interactions at the deposition hole wall. Average P- and S-wave amplitude change is presented in Figure 5-7 for these ray paths. The amplitude changes observed on these ray paths are significant and closely follow those observed through the rock alone. Although the results from these raypaths cannot be used to analyse changes in the rock, they could be used to analyse changes inside the deposition hole. In order to perform such an analysis would require full-waveform modelling of the deposition hole interior and pressure-temperature changes.

Figure 5-8 gives a measure of the number of located AEs. The frequency of located events during this reporting period is low compared to when temperature was increasing at a faster rate and when the rapid change in pressure occurred in December 2004. The low number of AEs suggests the rock mass has stabilised. Although the temperature during this period was high, it was fairly constant compared to previous monitoring (only changing  $2.2^{\circ}\text{C}$ ). The pressure measured in the deposition hole also increased to over 4.5MPa on one instrument from 3.3MPa at the start of this reporting period (equivalent to a rate of approximately 7kPa per day). This would lead to a confining pressure being placed on the rock around the deposition hole and explains the cessation in AEs as movement on macrofractures and microcracks is inhibited. This is supported by relatively constant measured velocities for much of this reporting period.

At the end of the reporting period there is a rapid decrease in temperature of the rock and pressure as the canister is turned off and drainage is opened. This appears to have little affect on the number, or distribution of AEs around the deposition hole, although the rate may be slowly accelerating at the end of the monitoring period. This differs to the results in December 2004 when a rapid pressure *increase* caused 32 events to locate in clusters over the course of two days. The events recorded then were interpreted as stress changes in the rock as it responds to the sudden pressure change. This induces small scale movement on pre-existing microcracks, or induces new microfractures in weaker volumes of the rock. In this case the pressure and temperature decrease has caused no redistribution of stresses sufficient to re-initiate further microfracturing.



**Figure 5-1:** P- and S-wave (a) velocity change and (b) amplitude change from the start of monitoring, plotted alongside temperature (TR6045) and pressure (PB616) measurements in deposition hole DA3545G01. The vertical blue lines represents the end of the previous reporting period and the start of this reporting period.



**Figure 5-2:** Average P- and S-wave velocity change for raypaths on category 'S1' together with temperature (TR6045) and total pressure (PB616) (top), Young's Modulus and Poisson's Ratio change (middle), and Crack Density and Saturation change (bottom).

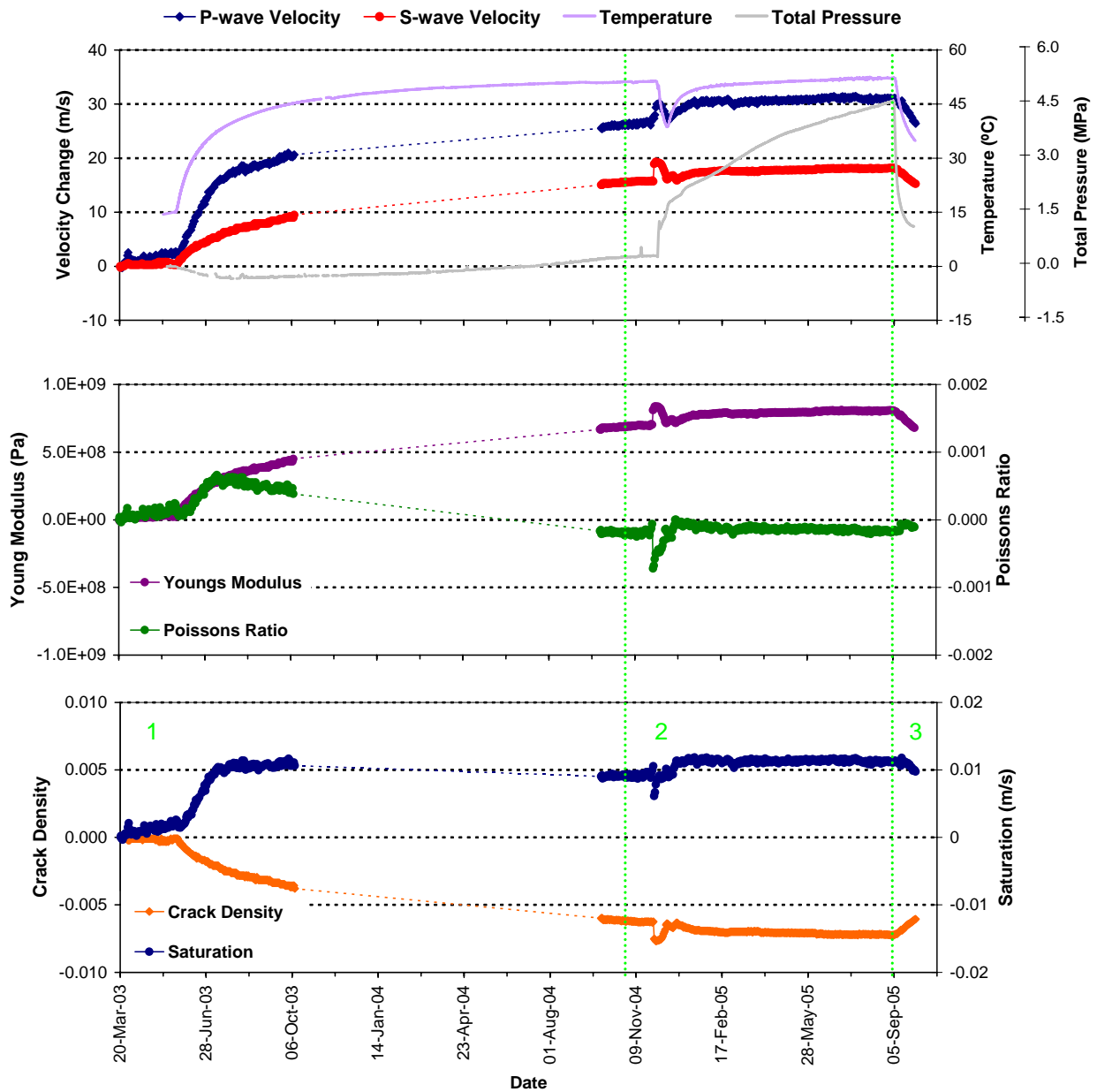


**Figure 5-3:** Average P- and S-wave velocity change for raypaths on category 'S3' together with temperature (TR6045) and total pressure (PB616) (top), Young's Modulus and Poisson's Ratio change (middle), and Crack Density and Saturation change (bottom).

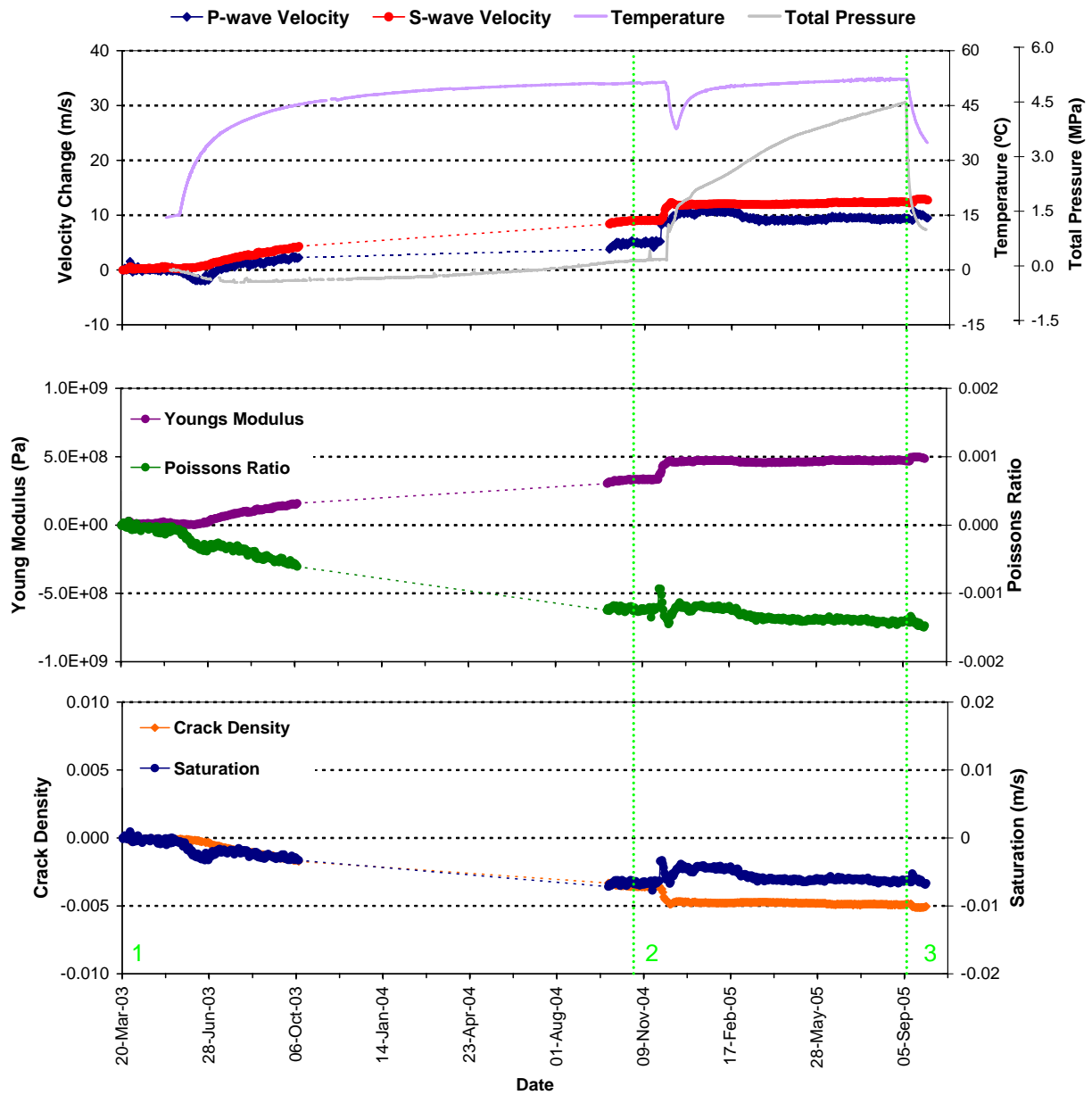


**Figure 5-4:** Average P- and S-wave velocity change for raypaths on category 'C1' together with temperature (TR6045) and total pressure (PB616) (top), Young's Modulus and Poisson's Ratio change (middle), and Crack Density and Saturation change (bottom).

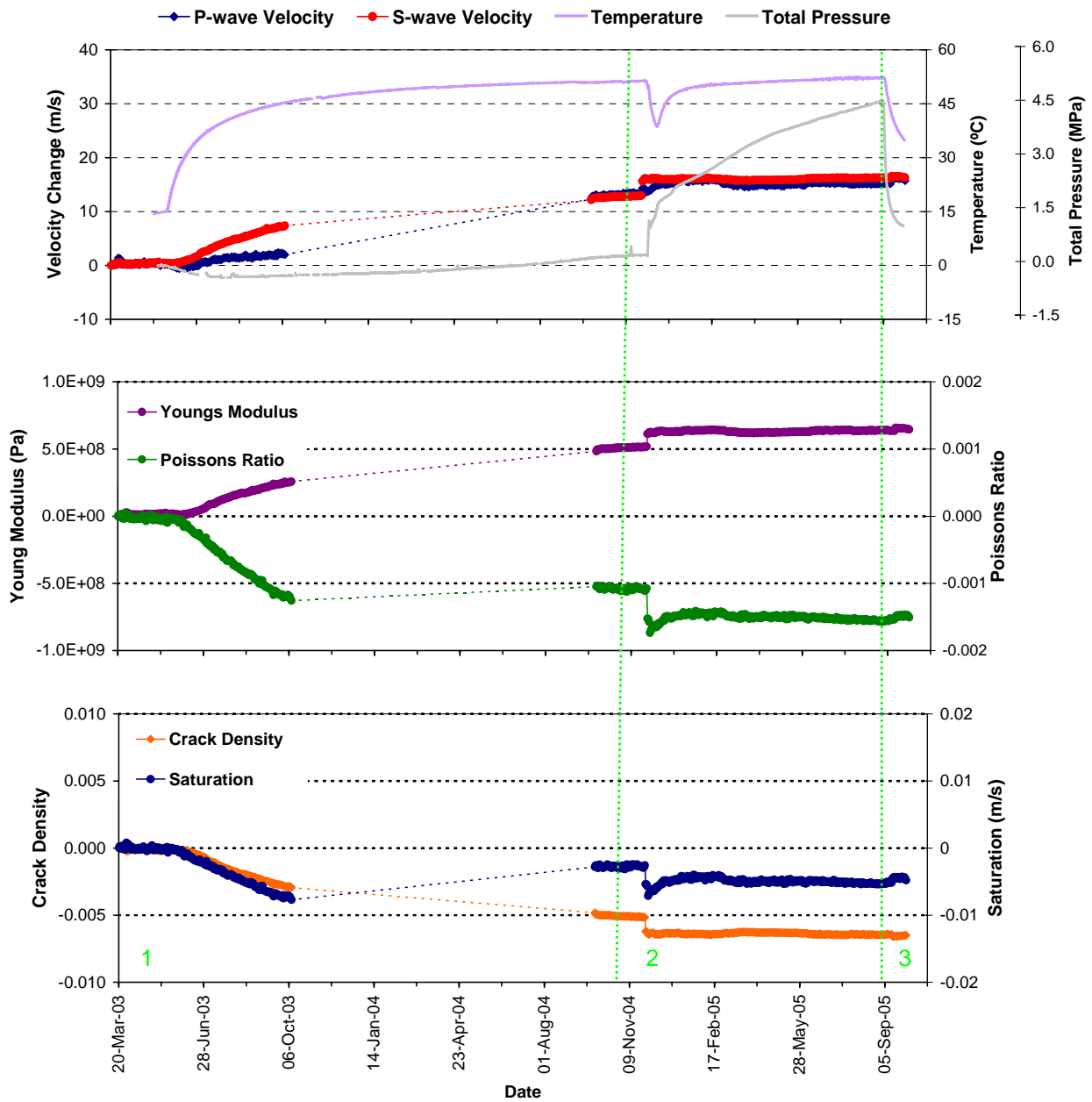


**Figure 5-5:** Average P- and S-wave velocity change for raypaths on category 'C2' together with temperature (TR6045) and total pressure (PB616) (top), Young's Modulus and Poisson's Ratio change (middle), and Crack Density and Saturation change (bottom).



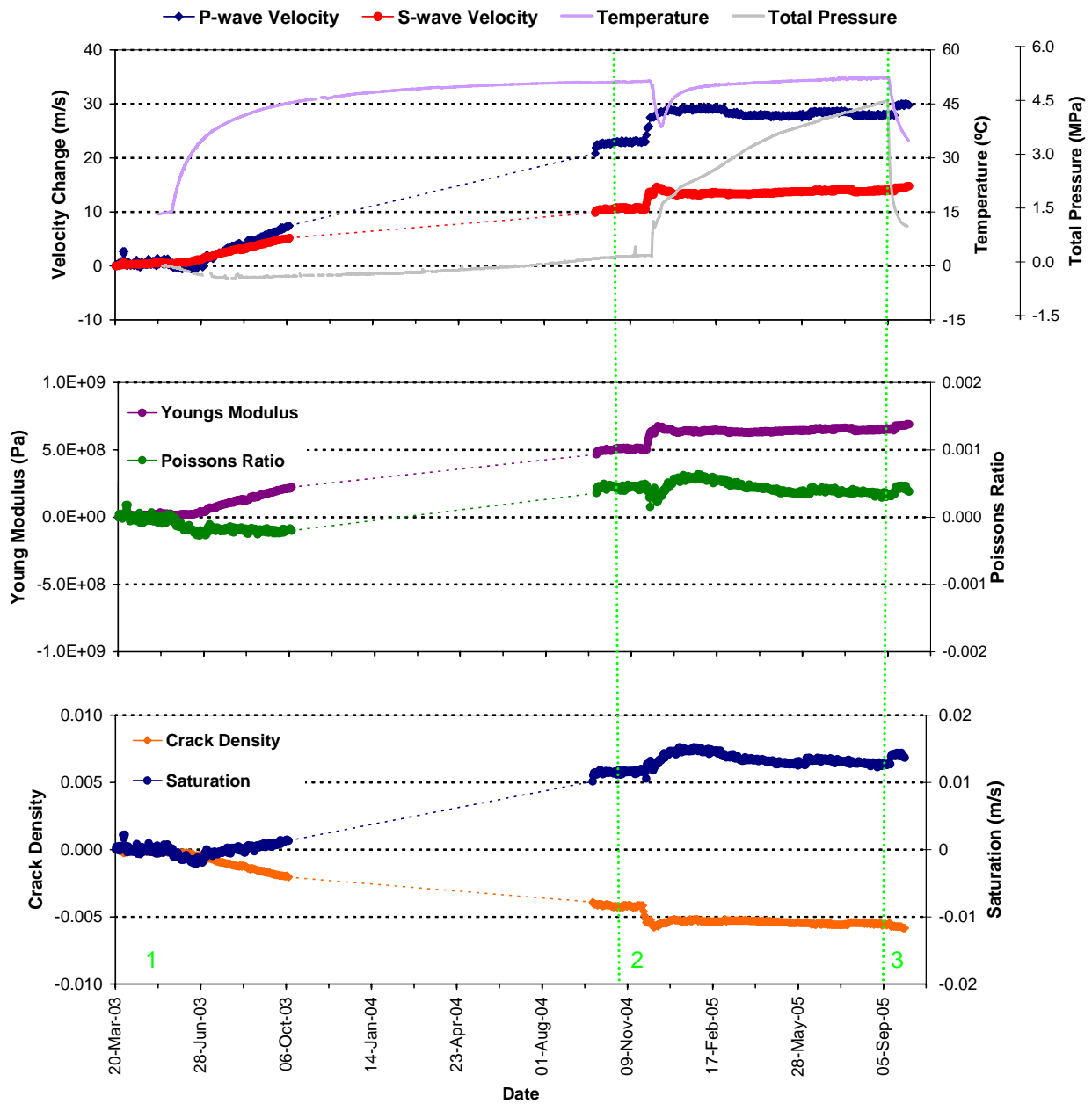


**Figure 5-6:** Average P- and S-wave velocity change for raypaths on category 'Far' together with temperature (TR6045) and total pressure (PB616) (top), Young's Modulus and Poisson's Ratio change (middle), and Crack Density and Saturation change (bottom).

**Table 5-1: Summary of velocity, amplitude and AE variation measured during three periods of temperature and/or pressure change.**

Name / Date	Temperature/Pressure	Velocity	Amplitude	AE
<p>PHASE 1</p> <p>25<sup>th</sup> May 2003 to 31<sup>st</sup> October 2004</p>	<p>Heaters in canister switched on causing an initially rapid change in temperature which gradually levels out to a constant increase. An increase of 35°C is measured for an instrument in rock adjacent to the deposition hole.</p> <p>Pressure constant</p>	<p>Rapid increase in P- and S-wave velocity on 'S3' category.</p> <p>Other categories show increases but to a lesser extent.</p> <p>Initial decrease in P-wave velocity in comparison to S-wave velocity for all raypaths except for 'S3'.</p>	<p>Amplitudes increase over this period by between 3dB and 9dB for P-wave amplitude, and 7dB and 12dB for S-wave amplitude.</p>	<p>AEs do not start immediately after heating. This could be a Kaise-type effect in which AE rate remains close to background level until stress increases above the largest previous value. Peak of 13 events located on 26<sup>th</sup> June 2003.</p>
<p>PHASE 2</p> <p>1<sup>st</sup> November 2004 to 4<sup>th</sup> September 2005</p>	<p>Drainage to tunnel closed on 1<sup>st</sup> November. Pressure in tunnel increases. Pressure increases measured in the buffer between 3<sup>rd</sup> and 5<sup>th</sup> December. Damage observed on canister on 6<sup>th</sup> December so drainage reopened and heaters switched off. Power switched on and drainage closed on 15<sup>th</sup> December.</p>	<p>Velocity increases measured close to the tunnel from 26<sup>th</sup> November.</p> <p>Larger increases measured on categories 'S1' and 'S3'.</p>	<p>Amplitude increases measured in the tunnel from 26<sup>th</sup> November.</p>	<p>Relatively large number of events recorded in this period. Peak rate of 32 AEs on 4<sup>th</sup> and 5<sup>th</sup> December.. Events locate in clusters in previously observed damage zone.</p>
<p>PHASE 3</p> <p>5<sup>th</sup> September 2005 to 30<sup>th</sup> September 2005</p>	<p>Drainage opened and heaters turned off on 5<sup>th</sup> September.</p>	<p>P- and S-wave velocities decrease on category 'S3' raypaths.</p> <p>Little velocity change measured on other categories.</p>	<p>P-wave amplitude decrease on all category raypaths.</p>	<p>Slight increase in event rate above background rate recorded in previous 5 months.</p>

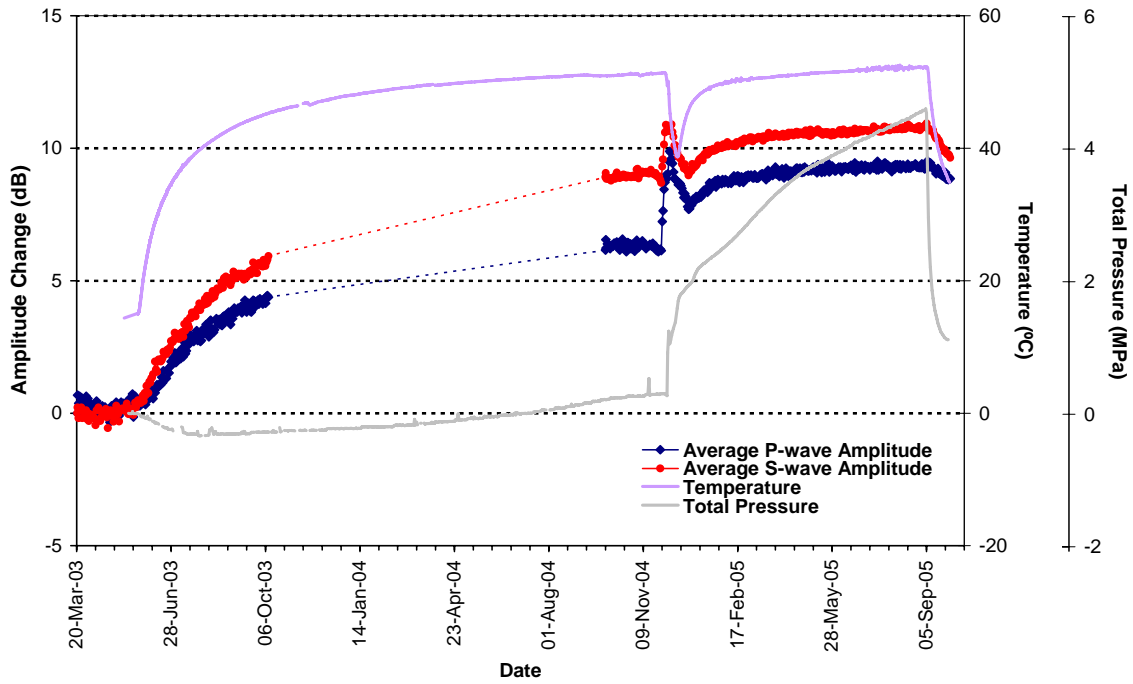


**Figure 5-7:** Average amplitude change for raypaths passing through the deposition hole, together with temperature (TR6045) and total pressure (PB616).

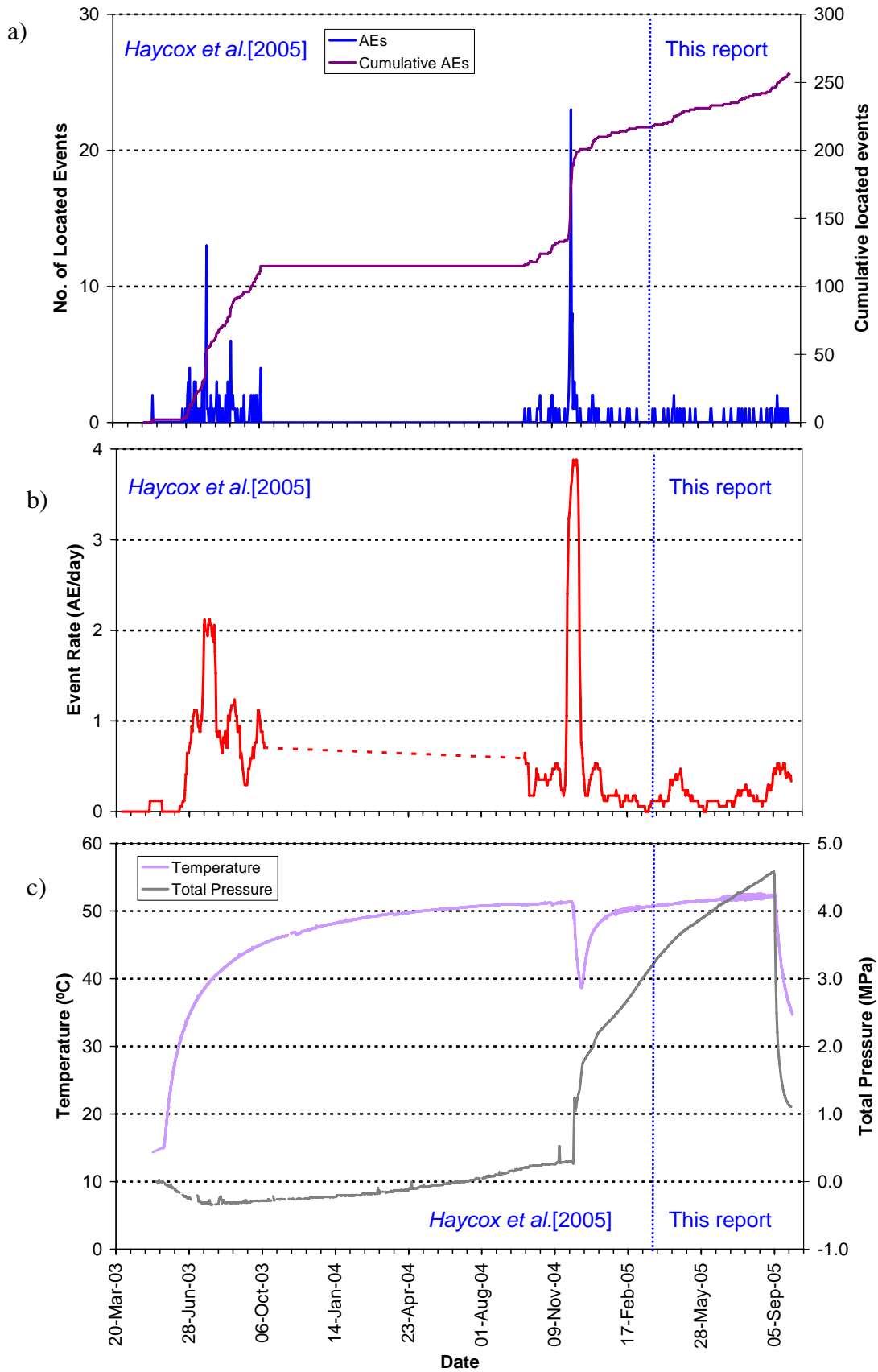


**Figure 5-8:** (a) Number and cumulative number of located events from the start of monitoring, (b) average number of AE events per day (averaged over 17 days) and (c) temperature (TR6045) and pressure (PB616) measurements in deposition hole DA3545G01.

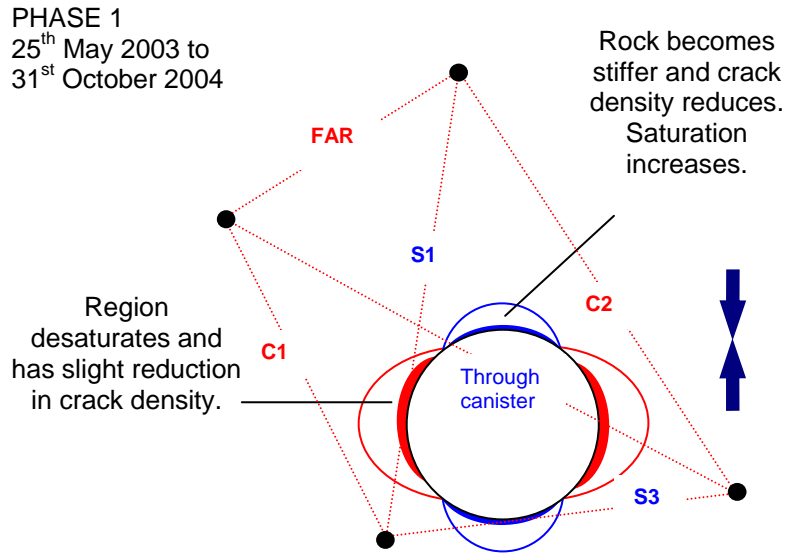


**Figure 5-9:** Schematic diagram of the deposition hole and explanation of changes experienced during Phase 1.

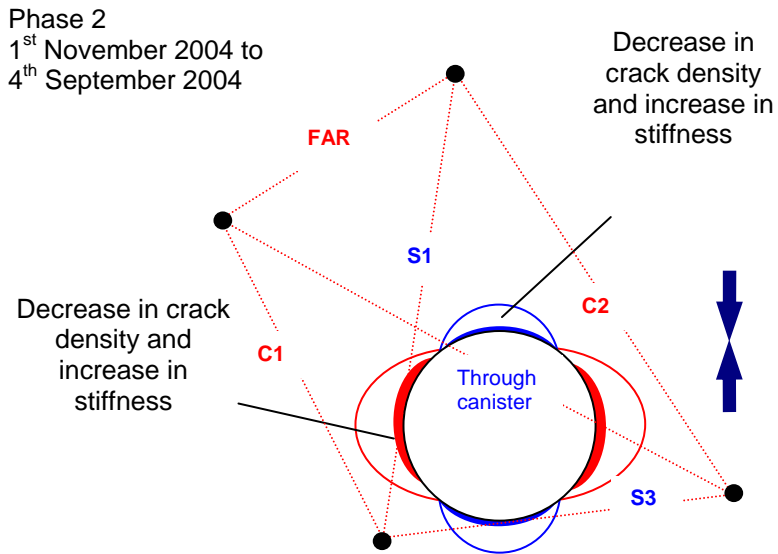


**Figure 5-10:** Schematic diagram of the deposition hole and explanation of changes experienced during Phase 2.

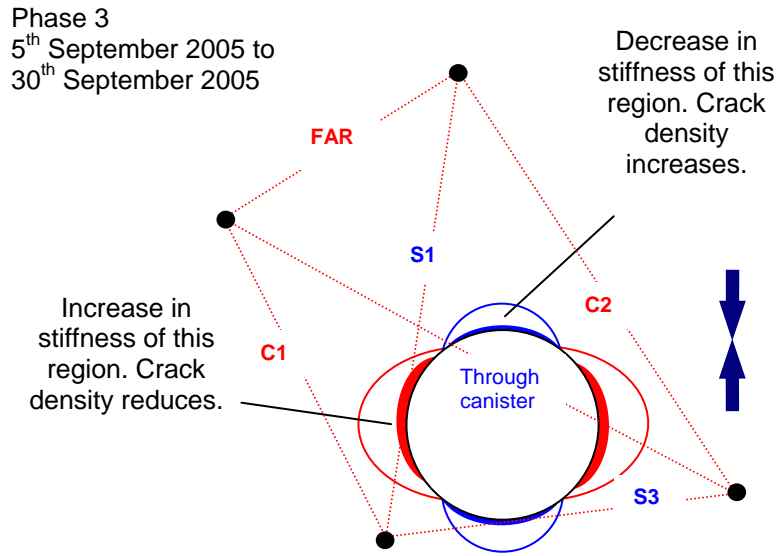


**Figure 5-11:** Schematic diagram of the deposition hole and explanation of changes experienced during Phase 3.

## 6 Results Summary and Conclusions

### 6.1 Overview

- This report describes results from acoustic emission (AE) and ultrasonic monitoring around a canister deposition hole (DA3545G01) in the Prototype Repository Experiment at SKB's Hard Rock Laboratory (HRL), Sweden. The monitoring aims to examine changes in the rock mass caused by an experimental repository environment, in particular due to thermal stresses induced from canister heating and pore pressures induced from tunnel sealing. Monitoring of this volume has previously been performed during excavation [*Pettitt et al.*, 1999a] and during the initial stages of canister heating and tunnel pressurisation [*Haycox et al.*, 2005]. This report is the first of an ongoing 6-monthly processing and interpretation of the results for the experiment and relates to the period between 1<sup>st</sup> April 2005 and 30<sup>th</sup> September 2005.
- The Prototype Repository Experiment has been designed to simulate a disposal tunnel in a real deep repository for disposal of high-level nuclear waste. Two techniques are utilised here to investigate the processes occurring within the rock mass around the deposition hole. AE monitoring is a 'passive' technique similar to earthquake monitoring but on a much smaller distance scale (source dimensions of millimetres). AEs occur on fractures in the rock when they are created or when they move. Ultrasonic surveys are also used to 'actively' examine the rock. In this case an array of transmitters sends signals to an array of receivers. Amplitude and velocity changes on the ray paths can then be used to examine changes in the rock's properties (Young's modulus, Poisson's ratio, Crack density and Saturation).
- AE and Ultrasonic monitoring has previously been conducted at the Prototype Repository during excavation of two deposition holes in Section II of the tunnel and when simulated canisters, installed in the deposition holes, were first heated and the tunnel pressurised. A summary of the key results from these monitoring periods is provided in Section 3. Monitoring is now continuing in 6-monthly reporting periods using a permanent ultrasonic array, with transducers installed into instrumentation boreholes in June 2002, before the tunnel was sealed. In April 2003 heaters in the simulated waste canisters were switched on causing temperatures to rapidly increase in the rock mass up to approximately 50°C at the rock wall. In November 2004 water drainage from the sealed Prototype tunnel was stopped causing a rapid increase in fluid pressures in the deposition hole.
- This report relates to the monitoring period starting 1<sup>st</sup> April 2005. During this period the temperature increases at a constant slow rate until 5<sup>th</sup> September 2005. After this date there is an exponential decrease consistent with the turning off of heaters in the deposition hole. Similarly, there is a trend of increasing pressure up to 5<sup>th</sup> September (an increase of 1.3MPa is observed on the deepest pressure instrument). This is followed by a rapid decrease in pressure coinciding with the date that drainage was re-opened to the Prototype Repository.

## 6.2 Ultrasonic Surveys

- Velocity changes are measured between transmitter-receiver pairs on the daily ultrasonic surveys using a cross-correlation technique that allows a velocity resolution of  $\pm 2\text{m.s}^{-1}$ . Relative to previous monitoring, there is only a small change in average velocity recorded during the monitoring period (averaged over all ray paths), with a general decrease observed when temperature and pressure starts to decrease. There is also a minor jump in average P-wave velocity of approximately  $1.3\text{m.s}^{-1}$  between the 13<sup>th</sup> and 14<sup>th</sup> September. This is not a large increase but is significant. Further investigation confirmed that it is a real change, and has been interpreted as a localized change in the general rock properties rather than the measurement devices used in the project. There is also a small jump in average S-wave velocity on the same date, although this is much smaller than the P-wave change. An analysis of crack density and saturation values, calculated from the velocity measurements, shows that the step in average velocities relates to a small but sudden change in saturation and is not so apparent in crack density. The jumps coincide with a period when pressure and temperature are both decreasing. This could be caused therefore by a sudden increase in fluid content of the rock mass as pressures and temperatures are removed, possibly by a shift in the conditions of the bentonite buffer within the deposition hole at this time.
- A variation is also observed in the average amplitude measurements during the time period. There is a general trend of increasing amplitude for most of the reporting period. This agrees closely with the constant rate of heating and pressure. A decrease in amplitude is then observed after 5<sup>th</sup> September 2005, which is very sensitive to the reduction in temperature and pressure. The decrease is more rapid than the increase recorded previously and tracks the temperature and pressure change. By the end of the reporting period, the P-wave amplitude was lower than at the start and the S-wave was slightly higher.
- The velocity results from individual ray paths show that the largest decreases during cooling and depressurisation are occurring on raypaths passing through a region of low compressive stress (or slightly tensile stress) defined by previous modelling of induced stresses. P-wave velocity shows a greater degree of variation than S-wave velocity. Overall the changes experienced are of low magnitude in comparison to changes occurring during the heating phase (up to 5<sup>th</sup> September). Amplitude changes are also relatively small during this reporting period. P-wave amplitudes are relatively constant until 5<sup>th</sup> September 2005, when there is a systematic decrease associated with the cooling and depressurisation. S-wave amplitudes increase slightly during the first part of the reporting period followed by a decrease that follows a similar trend to the P-waves.
- Calculated rock parameters (Young's Modulus, Poisson's Ratio, Crack Density and Saturation) show that ray paths that pass at distance from the deposition hole pass through rock that is relatively unaffected by the reduction in temperature and pressure. Greater variation is observed on raypaths that pass through regions of high and low compressive stress zones, close to the deposition hole wall. An increase in crack density is observed in the region of low compressive stress, which is interpreted as the opening of existing microfractures and pore spaces.



- Raypaths through the zone of high compressive stress show a decrease in saturation over the reporting period with little variation in crack density. This is a result of the measured decrease in P-wave velocity without a corresponding decrease in S-wave velocity and is interpreted as being caused by a drying of the rock mass in the zone experiencing high compressive stresses. During the period of cooling and de-pressurisation, saturation is observed to decrease on raypaths through zones of both the high and low compressive stress, possibly as a result of the combined effect of lowering fluid pressures whilst the rock remains relatively warm (>35°C).
- Significant differences have been observed in the response on raypaths passing through volumes of rock in states of high and low compressive stresses induced by the *in situ* stress field and the deposition hole void. Raypaths that pass through unloaded volumes of the rock mass record a much higher response and are more sensitive to thermal stresses, caused by changes in temperature, than ray paths that pass through loaded volumes. Changes in measured velocities and amplitudes, and calculated rock parameters, have been summarised for the entire monitoring since the start of heating. The measured changes are a result of the three-dimensional stress state of the rock around the deposition hole and the coupled nature of the pressure and temperature effects in the loaded and unloaded volumes. It's observed that since drainage from the Prototype Repository was closed in November 2004 pressure from within the deposition hole, caused by hydraulic pressure and swelling of the bentonite buffer, is the primary constraint on changes to properties of the rock around the deposition hole.
- Velocity measurements during the initial pressure rise describe an increase in the stiffness of the rock with a corresponding decrease in crack density. The magnitude increase is greater for ray paths that pass through volumes close to the deposition hole containing a higher proportion of microfractures in an excavation damage zone. The pressure increase acts as a confining pressure on the rock mass leading to a closure of the pre-existing microcrack fabric and so a reduction in crack density. We observe that only a relatively small pressure increase is sufficient to close this microcrack fabric in the volumes already under high compressive stresses, leading to an initially high rate of change in measured velocities followed by a constant level, even though pressures and temperatures may keep increasing afterwards. The required pressure increase is approximately 1.5MPa. Volumes of rock that have high compressive stresses, induced from the *in situ* stress field, and have high confining pressure from the deposition hole interior have a relatively closed microcrack fabric leading to a relative insensitivity to changing thermal stresses. When pressures are reduced in this monitoring period, the insensitivity remains due to the confining pressure remaining high. Volumes of rock that have low compressive stresses induced from the *in situ* stress field record a relatively high response to the change in temperature. The microcrack fabric in these volumes is relatively unconfined allowing the fabric to be reactive to an unloading of thermal stresses.

### 6.3 Acoustic Emissions

- Thirty-eight AEs have been located with high confidence from 82 triggered events recorded during this period. The rate of activity increases slightly in early September co-incident with the pressure and temperature decreases. The rate of

activity is slightly lower during this period (0.21 Events per day on average) compared to the previous six months of heating (0.32 Events per day on average after omitting the large pressure drop observed in that time period). The majority of the AEs locate in the immediate vicinity of deposition hole DA3545G01. Two events also locate close to the neighbouring deposition hole DA3551G01. A cluster of events is situated on the north-east side of deposition hole DA3545G01, at a depth of 457.2m just above the depth of the deposition-hole floor. Another cluster of events is observed at a depth of approximately 451.5m. In previous monitoring periods, the majority of events were distributed in the NE and SW quadrants which coincide with regions of increased compressive stress as imaged during excavation and initial stages of heating [Pettitt *et al.*, 2000; Pettitt *et al.*, 2002; Haycox *et al.*, 2005]. Smaller clusters were observed in orthogonal regions of low-compressive or tensile stress. The events observed here are consistent with these previous results with the small amount of clustering observed locating in regions of previous activity. The events are therefore interpreted as a continuation of activity in the previously imaged damage zone and, similar to during excavation and initial heating, are created either by movement on pre-existing microcracks, or as a result of extension or formation of new microcracks in the existing damaged region.

- Four events are located in the rock mass between the two deposition holes at between 455.3 and 455.7m depth. The events are believed to coincide with a semi-horizontal macroscopic fracture that is observed to intersect the deposition holes at this height [Pettitt *et al.*, 2000]. Three low-magnitude events were also observed along this fracture during the excavation phase [Pettitt *et al.*, 1999a] and 11 events were located during early stages of heating [Haycox *et al.*, 2005].
- The frequency of located events during this reporting period is low compared to when temperature was increasing at a faster rate and when the rapid change in pressure occurred in December 2004. The low number of AEs suggests the rock mass has stabilised. Until September 2005, the temperature has remained at a relatively steady level. Pressure from the deposition hole interior has increased to over 4.5MPa, which would lead to a confining pressure being placed on the rock around the deposition hole. This explains the cessation in AEs as movement on macrofractures and microcracks is inhibited by the confining pressure; a response observed in laboratory rock tests [Pettitt and Haycox, 2004], and in the Tunnel Sealing Experiment (TSX) at AECL's Underground Research Laboratory (URL) [Baker and Young, 2003].
- At the end of the reporting period there is a rapid decrease in temperature of the rock and pressure as the canister is turned off and drainage is opened. This appears to have little affect on the number, or distribution of AEs around the deposition hole, although the rate may be slowly accelerating at the end of the monitoring period. This differs to the results in December 2004 when a rapid pressure *increase* caused 32 events to locate in clusters over the course of two days. The events recorded then were interpreted as stress changes in the rock as it responds to the sudden pressure change. This induces small scale movement on pre-existing microcracks, or induces new microfractures in weaker volumes of the rock. In this monitoring period the pressure and temperature decrease has caused no redistribution of stresses sufficient to re-initiation further significant microfracturing.

## References

**Baker, C. and R.P. Young, 2002.** Acoustic emission and ultrasonic monitoring around the TSX tunnel clay and concrete bulkheads between October 2001 and October 2002. Ontario Power Generation, Nuclear Waste Management Division Report.

**Goudarzi, R. and L-E. Johannesson, 2004.** Sensor Data Report (Period: 010917-040901). Prototype Repository. Report No: 11, Swedish Nuclear Fuel and Waste Management Company, Sweden.

**Goudarzi, R., 2005.** Pers. Comm.

**Haycox, J.R., W.S. Pettitt, and R.P. Young, 2005,** Acoustic Emission and Ultrasonic Monitoring During the Heating of Deposition hole DA3545G01 in the Prototype Repository to March 2005. ASC report to Swedish Nuclear Fuel and Waste Management Company, Sweden.

**Johannesson, L-E., 2005.** Pers. Comm.

**Maxwell, S.C., and R.P. Young,** A controlled in-situ investigation of the relationship between stress, velocity and induced seismicity, *Geophys. Res. Lett.*, 22, 1049-1052, 1995.

**Patel, S., L.-O. Dahlstrom, and L. Stenberg,** Characterisation of the Rock Mass in the Prototype Repository at Äspö HRL Stage 1, Äspö Hard Rock Laboratory Progress Report HRL-97-24, Swedish Nuclear Fuel and Waste Management Company, Sweden, 1997.

**Pettitt, W.S., C. Baker, and R.P. Young,** Acoustic emission and ultrasonic monitoring during the excavation of deposition holes in the Prototype Repository, International Progress Report IPR-01-01, Äspö Hard Rock Laboratory, Swedish Nuclear Fuel and Waste Management Company, Sweden, 1999.

**Pettitt, W.S., C. Baker, and R.P. Young,** Analysis of the in-situ principal stress field at the HRL using acoustic emission data, International Progress Report IPR-01-09, Äspö Hard Rock Laboratory, Swedish Nuclear Fuel and Waste Management Company, Sweden, 2000.

**Pettitt, W.S., C. Baker, R.P. Young, L. Dahlstrom, and G. Ramqvist,** The assessment of Damage Around Critical Engineering Structures Using Induced Seismicity and Ultrasonic Techniques, *Pure and Applied Geophysics*, 159, 179-195, 2002.

**Pettitt, W.S., Baker, C., Collins, D.S., and R.P. Young, 2005.** InSite Seismic Processor – User Operations Manual Version 2.13. Applied Seismology Consultants Ltd., Shrewsbury, UK.

**Pettitt, W.S. and J.R. Haycox,** Acoustic emission observations of rock fracture under true-triaxial stress. In SAFETI Year 2 Progress Report, University of Liverpool, UK, 2004.

**SKB,** Äspö Hard Rock Laboratory: Current Research Projects 1998, Swedish Nuclear Fuel and Waste Management Company, Sweden, 1999.

**Telford, W.M., Geldart, L.P., and Sheriff, R.E.,** Applied Geophysics: Second Edition, Cambridge University Press, 1990.

**Young, R.P. and W.S. Pettitt,** Investigating the stability of engineered structures using acoustic validation of numerical models, in Geotechnical Special Publication No 102, edited by J.F. Labuz, S.D. Glaser, and E. Dawson, pp. 1-15, ASCE, USA, 2000.

**Zimmerman, R.W and M.S. King,** Propagation of acoustic waves through cracked rock, 20<sup>th</sup> Symposium on Rock Mechanics, Rapid City, SD, 1985.

# Appendix I      Methodology

## ***Data Acquisition***

The ultrasonic array consists of twenty-four ultrasonic transducers configured as eight transmitters and sixteen receivers installed into four instrumentation boreholes. The transducers are fixed into the boreholes using specially designed frames (Figure 6-1) – two transmitters and four receivers per frame. The boreholes are vertical, 76mm in diameter and approximately 10 meters in length distributed around each deposition hole volume. The array has been designed so as to provide good coverage for AE locations and to provide ‘skimming’ ray paths that pass within a few centimetres of the deposition-hole void so as to sample the rock immediately adjacent to the deposition-hole wall. The layout of the instrumentation boreholes is shown in Figure 6-2 and described further in Table 6-1. Each of the ultrasonic transducers has a hemispherical brass cap fixed over its active face and is then spring-loaded against the borehole surface so as to obtain good coupling to the rock mass. The boreholes have then been filled with a slightly expansive grout so as to permanently fix the transducers in place, reduce the likelihood of damage to the transducers and to remove the borehole voids.

The piezoelectric transducers operate by converting a transient elastic wave into an electric signal or visa versa. The monitoring system is then operated in one of two modes. The first is used to passively monitor AE activity preferentially within the array volume. AEs release elastic energy in the same way as 'earthquakes' but over a very small scale. At these frequencies AEs have a moment magnitude ( $M_w$ ) of approximately -6. They occur either during the creation process of new fractures within the medium, or on pre-existing fractures due to small scale movements. Each receiver has a frequency response of approximately 35-350kHz and contains a 40dB pre-amplifier. This minimises a reduction in signal-to-noise between the sensors and the acquisition system. The sensors have a vulcanised surround and a high pressure reinforced cable to protect them from water infiltration. In addition, polyamide tubes and *Swagelok* connectors have been fitted to the cables to reduce the likelihood of breakage.

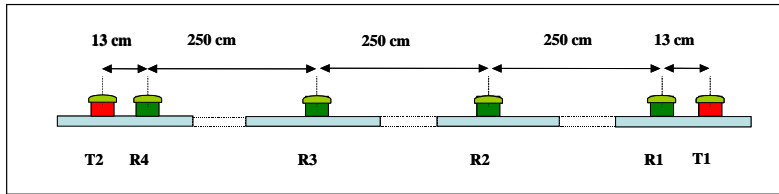


**Figure 6-1:** Top: Schematic diagram of the locations of all transducers on a single frame. Left: Photo of a section of the transducer assembly. Right: The transducer assembly during installation.

Figure 6-3 shows a schematic diagram of the acquisition system used. Cables from each transducer pass through the pillar between the PRT and the G-tunnel. Data acquisition uses a Hyperion Ultrasonic System controlled by a PC, set up within a cabin provided by SKB. This has 16 receiving channels and 8 transmitting channels. An AE is recorded when the amplitude of the signal on a specified number of channels exceeds a trigger threshold within a time window of 5ms. The system then records the full-waveform signals from all 16 transducers. In this case a trigger threshold of 50mV on three channels was used. This allows the system to have sufficient sensitivity to record high quality data without recording an abundance of activity that cannot be processed due to very small signal to noise on only a few channels. The captured signals are digitised with a sampling interval of  $1\mu\text{s}$  and a total length of 4096 data points. In general, low noise levels were observed ( $<2\text{mV}$ ) giving high signal to noise and good quality data. AE monitoring is set to switch off during daytime working hours (6am-8pm) so as to minimise the amount of noise recorded from human activity.

A second operating mode actively acquires ultrasonic waveforms by scanning across the volume. This allows measurements of P- and S-wave velocities and signal amplitudes over a possible 128 different ray paths. By repeating these ultrasonic surveys at increments in time, a temporal analysis is obtained for the variation in medium properties. Ultrasonic surveys are conducted daily at 1am in order to measure changes in P- and S-wave signals. At that time of night, no human activity will cause noise that can interfere with the signals received. A Panametrics signal generator is used to produce a high frequency electric spike. This is sent to each of the 8 transmitters in turn.

The signal emitted from each transmitter is recorded over the 16 receivers in a similar fashion to that described above. An external trigger pulse from the signal generator is used to trigger the acquisition system and identifies the transmission start time to an accuracy of one sample point. In order to decrease random noise the signal from each transmitter is stacked 100 times.

**Table 6-1: Boreholes used for AE monitoring of deposition hole DA3545G01.**

SKB Borehole designation	ASC Borehole reference	Transducer Numbers
KA3543G01	1	T1, T2, R1-R4
KA3545G02	2	T3, T4, R5-R8
KA3548G03	3	T5, T6, R9-R12
KA3548G02	4	T7, T8, R13-R16

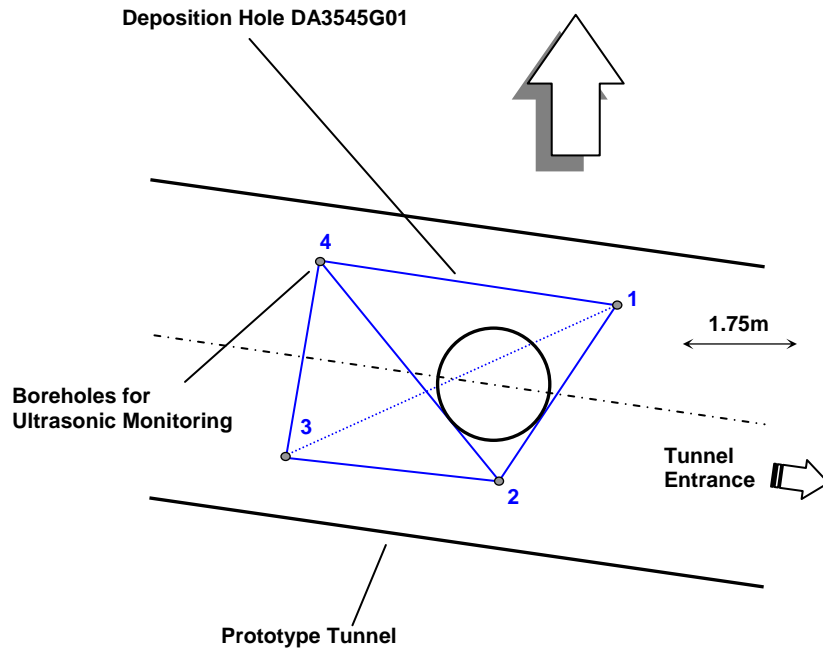


**Figure 6-2:** Plan view of the array geometry for Deposition Hole DA3545G01 during heating in the Prototype Tunnel. The blue solid lines represent direct raypaths between sondes illustrating their ‘skimming’ nature. The blue dashed line represents a raypath that travels through the deposition hole.

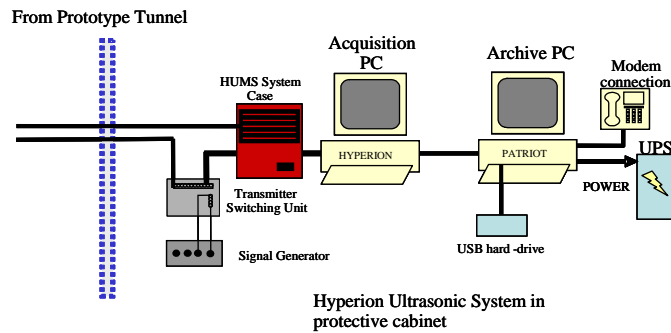


**Figure 6-3:** Schematic diagram of the hardware used for the heating stage in the Prototype Repository. The ultrasonic pulse generator sends a signal to each transmitter and the resulting signal is recorded on each receiver. The receivers are also used to listen for AE activity. The archive PC is required to make a copy of the data for backup purposes.

## Processing Procedure

### Overview

ASC's InSite Seismic Processor has been used to automatically process both the AE and ultrasonic survey data. Appendix 1A and Appendix 1B give the processing parameters used. *Pettitt et al.*[2005] provides a detailed description of this software.

### Ultrasonic Data Procedure

The ultrasonic survey full-waveform data was initially stored with the AE data. This was automatically sorted and the survey data extracted to a separate processing project. A 'reference' survey from the previous monitoring period was used, and imported into the project. The P- and S-wave arrivals were manually picked during the previous monitoring period. Knowing the transmitter and receiver locations, the ultrasonic velocity for each ray path was calculated with an estimated uncertainty of  $\pm 30 \text{m.s}^{-1}$  ( $\pm 3$  data points). A cross-correlation procedure was then used to automatically process subsequent surveys. This technique cross-correlates P- and S-wave arrivals from a transmitter-receiver pair with arrivals recorded on the same transmitter-receiver pair on the reference survey. This results in high-precision measurements of P- and S-wave velocity change with estimated uncertainties of  $\pm 2 \text{m.s}^{-1}$  between surveys. Note that when the transmitter and receiver are on the same borehole, the raypath is not used due to the introduction of transmission effects from the instrumentation borehole, grout and transducer frames.

The main reason for the reduction of uncertainty when using the cross-correlation procedure is the dependency of manual picking on the user's judgement of the point of arrival. This can usually be quite indiscriminate because of random noise superimposed on the first few data points of the first break. Additionally, the procedure is run automatically without any loss of precision resulting in efficient waveform processing. The cross-correlation procedure then allows for a high-resolution analysis to be performed and hence small changes in velocity to be observed. This is extremely important when changes in rock properties occur over only a small section (5%) of the ray path.



Figure 6-4 gives example waveforms recorded from one of the transmitters during this reporting period. Each waveform is first automatically picked to obtain an estimate of the P-wave or S-wave arrival. A window is then automatically defined around the arrival and a bell function is applied, centred on the automatic pick. The data at the ends of the window then have a much smaller effect on the cross-correlation. The windowed data is then cross-correlated [Telford *et al.*, 1990] with a similar window constructed around the arrival on the reference survey. The change in arrival time is then converted to a change in velocity knowing the manually-picked arrival time for the reference survey. Waveforms that do not provide automatic picks are not cross-correlated. This gives an automatic discrimination of signals that have very poor signal to noise ratios and could give spurious cross-correlation results from poor discrimination of the first arrival. During the automatic processing an arrival amplitude is also calculated from within a processing window defined by a minimum and maximum transmission velocity. This provides a robust measure of arrival amplitudes between surveys.

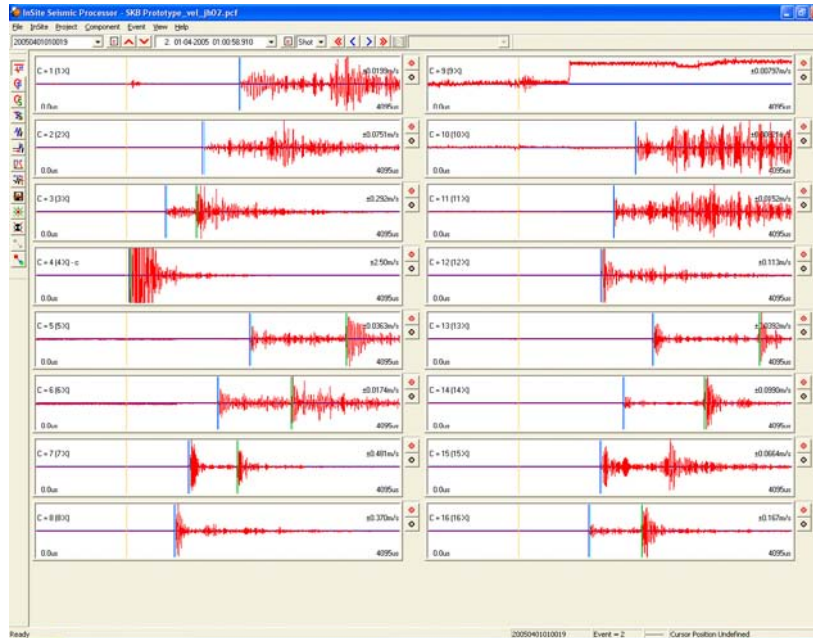


**Figure 6-4:** Waveforms recorded from one transmitter on the array of sixteen receivers. The gold markers indicate the transmission time. The blue and green markers indicate picked P- and S-wave arrivals respectively.

When calculating average velocities and amplitudes, raypaths passing through the deposition hole are removed due to the uncertain transmission paths produced by the wave travelling in the rock around the deposition hole and through the bentonite, fluid and canister fill. Therefore the majority of raypaths between boreholes 1 and 3 (transmitters 1, 2, 5, 6 and receivers 1, 2, 3, 4) are not used in the analysis. An exception is made for the deepest raypaths that pass under the deposition hole entirely through rock. Raypaths that pass through the deposition hole are still processed and an analysis of the results can be found in Section 5.

The dynamic Young's modulus  $E$ , and dynamic Poisson's Ratio,  $\nu$ , can be calculated from the velocity measurements using Equation 1 and Equation 2

$$E = \rho V_s^2 \left( \frac{3V_p^2 - 4V_s^2}{V_p^2 - V_s^2} \right) \quad \text{Equation 1}$$

$$\nu = \frac{V_p^2 - 2V_s^2}{2(V_p^2 - V_s^2)} \quad \text{Equation 2}$$

$V_p$  and  $V_s$  values are also used to model for crack density ( $c$ ) and saturation ( $s$ ) in the rock mass using the method of *Zimmerman and King*[1985]. The crack density parameter is defined by the number of cracks (penny-shaped) per unit volume multiplied by the mean value of the cube of the crack radius (Equation 3). This method assumes the elastic modulus  $E$  and  $\nu$  in the damaged material normalized to the undisturbed material, decrease exponentially with crack density. Also assumed are the shear modulus ( $\mu$ ) is unaffected by  $s$ , and the bulk modulus ( $k$ ) increases linearly with  $s$ , equalling that of uncracked rock when  $s=1$ . Equation 4 shows the calculation used to determine saturation.

$$c = \frac{9}{16} \ln \left( \frac{2\mu}{E_0 - 2\mu\nu_0} \right) \quad \text{Equation 3}$$

$$s = \frac{k(c, s) - k(c, 0)}{k_0 - k(c, 0)} \quad \text{Equation 4}$$

The calculations require an estimation of the completely undisturbed rock (i.e. an unsaturated, uncracked, intact rock mass). This study assumes values of  $V_{OP} = 6660 \text{m.s}^{-1}$ , and  $V_{OS} = 3840 \text{m.s}^{-1}$  for the undisturbed material taken from laboratory tests on a similar granite, summarized in *Maxwell et al.*[1998]. A value of  $2650 \text{kg m}^{-3}$  is presented by *Pettitt et al.*[2002] for the density of the rock mass.

The calculations of Young's Modulus and Poisson's ratio from measured velocities makes an assumption of an isotropic elastic medium. Under this assumption a rock can be completely characterised by two independent constants. One case of an isotropic elastic medium is a rock with a random distribution of cracks embedded in an isotropic mineral matrix. Under the application of a hydrostatic compressive stress, the rock will stay isotropic but become stiffer (which will become characterised by increased velocity  $V_p$ ,  $V_s$  and therefore increased Young's modulus). In contrast, under the application of a uniaxial compressive stress, cracks with normal's parallel or nearly parallel to the applied stress will preferentially close and the rock will take on a transversely isotropic symmetry. Under this situation P- and S-wave velocities become variable with orientation. The crack density and saturation calculations also assume an isotropic elastic medium.

It should be noted that  $E$  and  $\nu$  calculated in this report are dynamic measurements due to the small strains exerted on the rockmass at high frequencies from the passing ultrasonic waves. Static  $E$  and  $\nu$  measurements, made from uniaxial laboratory tests on rock samples, may be different from dynamic values – even if sample disturbance is minimal – due to the larger strains exerted over relatively long periods of time.

## **Acoustic Emission Procedure**

The procedure used to process the AEs in this reporting period has been undertaken as follows:

1. Calibration surveys from the installation phase (when the deposition hole was open) have been used to optimise an automatic picking and source location algorithm and check location uncertainties. ASC's InSite seismic processing software was used for location and visualisation.
2. Where possible, P- and S-wave arrival times were measured for each AE using the automatic picking procedure.
3. AEs with  $\geq 6$  P-wave arrival times were input into a downhill-simplex location algorithm [Pettitt *et al.*, 2005]. This has the option of incorporating either a three-dimensional anisotropic velocity structure or an isotropic structure. Velocities calculated from the ultrasonic surveys were used.
4. The waveforms from all events were visually inspected to ensure they were 'real' acoustic emissions. Events were removed if they had the appearance of noise spikes (increase in amplitude is recorded on all channels at the same time) or they were the result of human noise (long period events that occur at close intervals during the day).
5. The acoustic emissions that remained had their arrivals manually picked to obtain the best possible location. Any events that located outside the expected region of activity were further checked to ensure accuracy. Experience from previous studies around deposition holes showed that large source location errors were produced if significant portions of a ray path passed through the excavated deposition hole void. This only becomes a problem for the largest AEs. AEs were reprocessed with these ray paths removed.
6. Finally, a filter was applied to remove all AEs with a location error greater than 1.0.

During the equipment installation phase, calibration shots have been undertaken to assess the sensitivity of the system to 'real' AEs and to determine the accuracy with which real events could be subsequently located by the array of sensors. A series of test 'shots' were performed on the wall of deposition hole DA3545G01 (Figure 6-5). The shots consisted of undertaking 10 'pencil lead breaks' and 10 hits with a screw-driver at 1 metre intervals down 4 lines along the deposition hole wall. The pencil-lead tests involved breaking the 0.5 mm lead from a mechanical pencil against the borehole wall. This is a 'standard' analogue for an AE as it generates a similar amount of high-frequency energy. An example of a pencil lead break test is shown in Figure 6-6. This was made at 6 metres below the tunnel surface on the deposition hole wall at a point adjacent to borehole KA3548G02. This corresponds to an AE source dimension on the millimetre scale (grain size).

The screw-driver hits provided a good amplitude signal for assessing the accuracy with which events can be located within the volume surrounded by the array. Figure 6-5 shows the results from one processed set of locations for a line of shots down the deposition hole wall. This shows that the array is able to locate events with good accuracy and consistency within an estimated uncertainty of approximately 10cm.

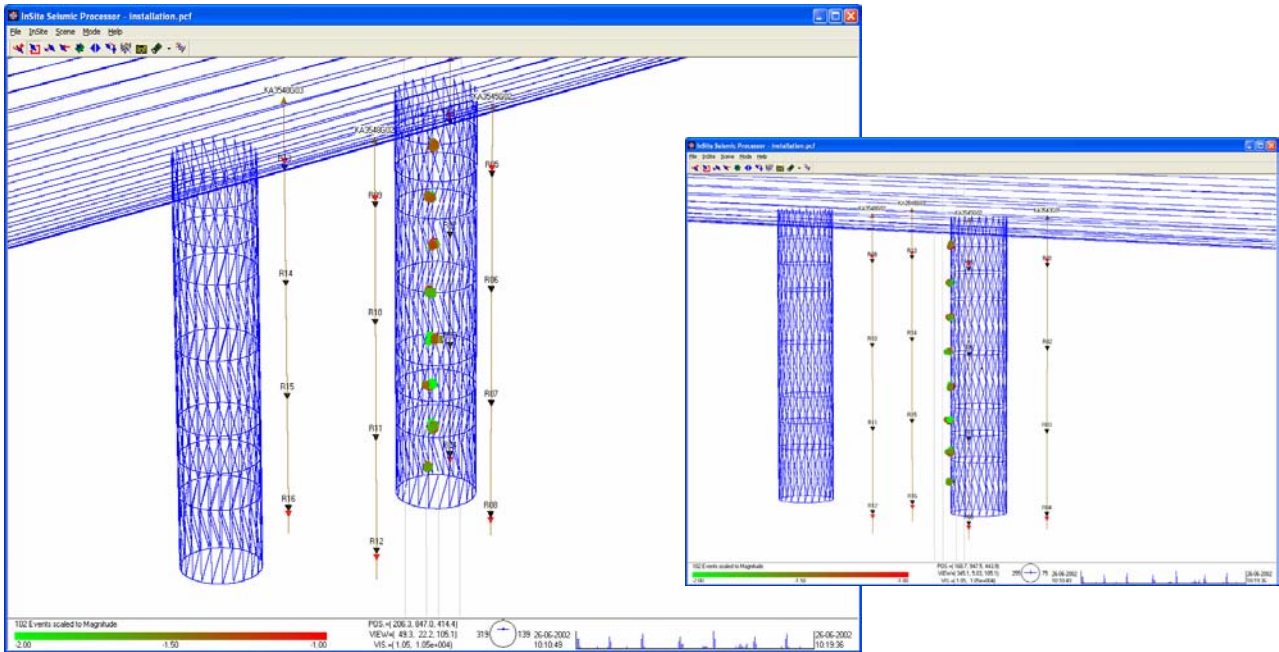


*Figure 6-5: Locations of calibration shots obtained from a series of tests at 1 metre intervals down the wall of deposition hole DA3545G01. The two views show that these line up and are located close to the surface of the hole.*

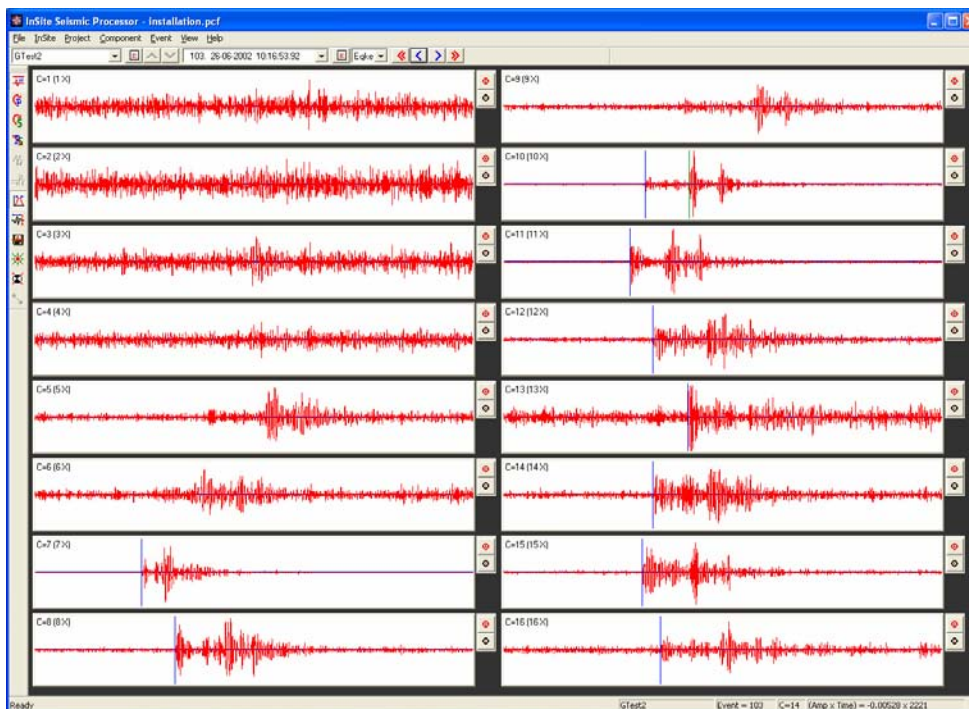


*Figure 6-6: Example waveforms from each of the 16 receiving channels for a `pencil-lead break` test undertaken against the Deposition hole (DA3545G01) wall 6 metres below the tunnel floor.*

## Appendix II Processing Parameters

### *Ultrasonic survey processing parameters:*

#### PROCESSING PARAMETERS

#### Velocity survey processing

<b>EVENT INITIALISATION</b>	
View/process waveforms by	Channel
Channel-view Width-to-height ratio	6
Waveform Response type	Set from sensor
Sampling time	1
Time units	Microseconds
Pre-signal points	200
Spline sampling time	0.2
Waveform To point	1023
P-Time correction	0
S-Time correction	0
Automatically update Channel Settings	NOT SET
Project Files	NULL

<b>AUTO PICKING</b>	
Allow P-wave-autopicking	YES, Use first peak in the auto-pick function
Back-window length	100
Front-window length	35
Picking Threshold	4
Min. Peak-to-Peak amplitude	0
Allow S-Wave Autopicking	YES, Use first peak in the auto-pick function
Back-window length	100
Front-window length	35
Picking Threshold	5
Min. Peak-to-Peak amplitude	0
Allow Automatic Amplitude Picking	YES
Use Velocity Window Picking	YES
P-wave Min. Velocity/Max. Velocity	4500, 6500
S-wave Min. Velocity/Max. Velocity	2500, 3500

<b>CROSS-CORRELATION</b>	
CCR Events	Referenced to a Survey
Reference Component	20041208005920
Reference Event	NULL
Window construction method	Front to Back
Window comparison method	Fixed to reference picks
Window Parameters	Back-window length = 20 Front-window length=30 Rise-time multiplier = NULL Power to raise waveform =1 Split to a Spline function = YES Obtain absolute waveform= NOT SET

<b>LOCATER</b>	<b><i>(not used in velocity surveys)</i></b>
Method	SIMPLEX INTO GEIGER
Method settings Simplex settings       Geiger settings	Tolerance = 0.01 LPNorm = 1 P-wave weighting = 1 S-wave weighting = 1 Use Outlier Identification = NOT SET Arrival error factor = x2 Tolerance (Loc. units) = 0.01 Step size (Loc.units) = 0.1 Max. Iterations = 100 Conditional No. Limit = 10000000000
Velocity Structure	Homogeneous Isotropic
Velocity Structure settings	P-wave velocity = 5973.85 m.s <sup>-1</sup> S-wave velocity = 3342.705 m.s <sup>-1</sup> Attenuation = 200 Q(S) value = 100
Data to use	P-wave Arrivals Only
Distance units	Metres
Working time units	Microseconds
Min P-wave arrivals	0
Min S-wave arrivals	0
Min Independent arrivals	5
Max. Residual	20
Start point	Start at the centroid of the array
Write report to RPT	NOT SET
Source parameters	Set to calculate automatically

## **AE processing parameters:**

### **PROCESSING PARAMETERS**

### **AE processing**

<b>EVENT INITIALISATION</b>	
View/process waveforms by	Channel
Channel-view Width-to-height ratio	6
Waveform Response type	Set from sensor
Sampling time	1
Time units	Microseconds
Pre-signal points	200
Spline sampling time	0.2
Waveform To point	1023
P-Time correction	0
S-Time correction	0
Automatically update Channel Settings	SET
Project Files	NULL

<b>AUTO PICKING</b>	
Allow P-wave-autopicking	YES, Use max peak in the auto-pick function
Back-window length	100
Front-window length	35
Picking Threshold	5
Min. Peak-to-Peak amplitude	0
Allow S-Wave Autopicking	YES, Use max peak in the auto-pick function
Back-window length	100
Front-window length	35
Picking Threshold	5
Min. Peak-to-Peak amplitude	0
Allow Automatic Amplitude Picking	NOT SET
Use Velocity Window Picking	YES
P-wave Min. Velocity/Max. Velocity	4500, 6500
S-wave Min. Velocity/Max. Velocity	2500, 3500

<b>CROSS-CORRELATION</b>	<b><i>(not used in AE processing)</i></b>
CCR Events	NOT SET
Reference Component	NOT SET
Reference Event	NULL (not activated)
Window construction method	Individual
Window comparison method	Fixed to reference picks
Window Parameters	Back-window length = 31 Front-window length = 31 Rise-time multiplier = NULL Power to raise waveform = 1 Split to a Spline function = NOT SET Obtain absolute waveform = NOT SET

<b>LOCATER</b>	
Method	SIMPLEX INTO GEIGER
Method settings Simplex settings	Tolerance = 0.01 LPNorm = 1 P-wave weighting = 1 S-wave weighting = 1 Use Outlier Identification = NOT SET Arrival error factor = x2
Geiger settings	Tolerance (Loc. units) = 0.01 Step size (Loc.units) = 0.1 Max. Iterations = 100 Conditional No. Limit = 10000000000
Velocity Structure	Homogeneous Isotropic
Velocity Structure settings	P-wave velocity = 5985 m.s <sup>-1</sup> S-wave velocity = 3343 m.s <sup>-1</sup> Attenuation = 200 Q(S) value = 100
Data to use	P-wave Arrivals Only
Distance units	Metres
Working time units	Microseconds
Min P-wave arrivals	0
Min S-wave arrivals	0
Min Independent arrivals	5
Max. Residual	20
Start point	Sart at the centroid of the array
Write report to RPT	NOT SET
Source parameters	Set to calculate automatically

<b>EVENT FILTER</b>	
Date and Time	NOT SET
Location volume	Minimum = (235, 880, 420) Maximum = (300, 964, 463)
L. Magnitude	NOT SET
Location Error	1
Independent Instruments	Minimum = 0

<b>SOURCE PARAMETERS</b>	
Automatic source-parameter windows	P-wave back window = 10 P-wave front window = 50 S-wave back window = 10 S-wave front window = 50
Source parameter calculations	Min number to use = 3
Automatic source-parameter windows	Apply Q correction = SET Source density = 2640 Source shear modulus = 39131400000 Av. radiation coefficient: Fp = 0.52 ,Fs = 0.63
Source parameter calculations	Source coefficient: kp = 2.01 , ks = 1.32
Magnitude calculations	Instrument magnitude = 1 * log (ppV) +0 Moment magnitude = 0.666667 * log(Mo) + -6